NASA Technical Memorandum 106233
AIAA–93–2162

Small Hydrogen/Oxygen Rocket Flowfield Behavior From Heat Flux Measurements

B.D. Reed
Lewis Research Center
Cleveland, Ohio

Prepared for the
29th Joint Propulsion Conference and Exhibit
cosponsored by the AIAA, SAE, ASME, and ASEE
Monterey, California, June 28–30, 1993

NASA

SMALL HYDROGEN/OXYGEN ROCKET FLOWFIELD BEHAVIOR FROM HEAT FLUX MEASUREMENTS

Brian D. Reed
NASA-Lewis Research Center
Cleveland, Ohio 44135

Abstract

The mixing and heat transfer phenomena in small rocket flowfields with fuel film cooling is not well understood. This study used an instrumented, water-cooled chamber with a gaseous hydrogen/gaseous oxygen injector to gather steady-state inner and outer wall temperature profiles. The chamber was tested at 414 kPa (60 psia) chamber pressure, from mixture ratios of 3.41 to 8.36. Sixty percent of the fuel was used for film cooling. These temperature profiles were used as boundary conditions in a finite element analysis program, MSC/NASTRAN, to calculate the local radial and axial heat fluxes in the chamber wall. The normal heat fluxes were then calculated and used as a diagnostic of the rocket's flowfield behavior. The normal heat fluxes determined for this study were on the order of 1.0 to 3.0 MW/m^2 (0.6 to 1.8 Btu/sec-in^2). In the cases where mixture ratio was 5 or above, there was a sharp local heat flux maximum in the barrel section of the chamber. This local maximum seems to indicate a reduction or breakdown of the fuel film cooling layer, possibly due to increased mixing in the shear layer between the film and core flows. However, the flow was thought to be completely laminar, as the throat Reynolds numbers were below 50,000 for all the cases in this study. The increased mixing in the shear layer in the higher mixture ratio cases appeared not to be due to the transition of the flow from laminar to turbulent, but rather due to increased reactions between the hydrogen film and oxidizer-rich core flows.

Nomenclature

Btu / sec in^2	British thermal unit per second per square inch	MW / m^2	megawatts per square meter
Btu / sec in °F	British thermal unit per second per inch per degrees Fahrenheit	N	Newton
°C	degrees Celsius	$\vec{n}$	normal vector
Cg	heat transfer contour coefficient	Pr	Prandtl number = $C_p\mu/k$
cm	centimeter	psia	pound force per square inch
C_p	specific heat	$\dot{q}''$	heat flux
C*	characteristic exhaust velocity	$\dot{q}_n''$	normal heat flux
D	chamber diameter	$\dot{q}_R''$	radial heat flux
°F	degrees Fahrenheit	$\vec{q}_T$	total heat flux vector
g	enthalpy difference heat transfer coefficient	$\dot{q}_z''$	axial heat flux
h	temperature difference heat transfer coefficient	R	radial position
H_{aw}	adiabatic wall enthalpy	r_c	recovery factor
H_R	reference enthalpy	Re	Reynolds number = $4\dot{m}/\pi\mu D$
H_{wall}	gas flow enthalpy at wall	St	Stanton number = $g/\rho u$
H_∞	static gas flow enthalpy	T_{aw}	adiabatic wall temperature
$H_{0\infty}$	stagnation gas flow enthalpy	T_{wall}	wall temperature
in	inch	u	gas flow axial velocity
k	gas flow thermal conductivity	W / (m °C)	Watts per meter per degrees Celcuis
kPa	kilopascal	Z	axial position
lbf	pound force	θ	normal angle
$\dot{m}$	mass flowrate	μ	gas flow viscosity
MR	mixture ratio	ρ	gas flow density

Introduction

Most space missions use low thrust propulsion for functions such as apogee insertion, attitude control, stationkeeping, rendezvous, docking, separation, midcourse correction, and planetary retro. Currently, the bulk of low thrust propulsion functions are provided by small chemical rockets with thrust levels, depending on the function, ranging from 450 mN (0.1 lbf) to 4500 N (1000 lbf). Monopropellant hydrazine and the bipropellant combination of monomethylhydrazine and nitrogen tetroxide are the most common propellants in use today for low thrust propulsion systems, with the hydrazine/nitrogen tetroxide combination gaining favor.[1] Liquid oxygen with a space storable fuel[2] (hydrazine, hydrocarbons) and the hydrogen/oxygen combination[3] are among the options for future low thrust propulsion systems.

The flowfields in small rockets differ from the larger thrust class rockets in several ways. With low chamber pressures (under 690 kPa (100 psia)), relatively small size (throat diameters under 2.54 cm (1 inch)) and a corresponding large surface-to-volume ratio, small rocket flows generally have Reynolds numbers well under 100,000 and may be strongly influenced by viscous effects. A substantial percentage of fuel is often required for film cooling of the walls in small rockets, particularly for radiation-cooled rockets, to keep the wall material below its thermal limits and to minimize heat soakback to the front end. The low Reynolds number flow and large amounts of fuel film cooling can lead to significant mixing and boundary layer losses in small rockets. Furthermore, in the mixing or shear layer a secondary combustion zone may exist between the fuel film cooling flow and the oxidizer-rich core flow. The behavior of this combusting shear layer between the film and core flows in small rockets is not well understood. Flows with liquid film cooling are even more complex, with a liquid film decomposing and vaporizing at some undetermined point in the chamber. This chemically-reacting, viscous-dominated flowfield has been, in part, responsible for the known difficulty of prediction of performance and thermal behavior in small rockets.[4]

To better understand and more accurately model the mixing and heat transfer phenomena in small rockets, an effort has been undertaken to gather local and global data on small rocket flowfields and to apply numerical models developed in the aeronautical community to rocket flowfield modeling. A suite of laser-based diagnostics, including Rayleigh and Raman spectroscopy, have been used to measure gas temperature, density, and velocity profiles in small rocket plumes.[5,6,7] Using optically-accessible combustion chambers, Raman spectroscopy will be used to measure species concentrations, gas temperatures, and flow velocity profiles near the injector and laser-induced fluorescence used to visualize the shear layer mixing process.[1] A diagnostic thruster instrumented with thermocouples and pressure transducers is being used to investigate differences in injectors and nozzle contours for small rockets.[8] A numerical code that models the full Navier-Stokes and species transport equations, originally developed to model supersonic combustion of hydrogen in air, has been adapted to model small rocket flowfields.[9,10,11]

This study used an instrumented, water-cooled, axisymmetric chamber with a gaseous hydrogen/gaseous oxygen injector to gather steady-state wall temperature profiles over a range of mixture ratios. These temperature profiles were used as boundary conditions in a finite element analysis program, MSC/NASTRAN, to calculate the local radial and axial heat fluxes in the chamber. Normal heat flux was then calculated as the dot product of the total heat flux and normal vectors. In this study, heat flux was used as a small rocket flowfield diagnostic - the objective was not to find absolute heat flux values (which would change for differing wall conditions), but rather to use heat flux as an indicator of fundamental characteristics of the flowfield over a range of mixture ratios.

Rocket Heat Transfer Studies

Rocket heat transfer studies have been conducted since the 1950's, although the majority of this work has been concerned with medium to launch thrust class engines. A summary of several heat transfer studies appears in reference 12. Many a priori heat transfer predictions were made with the assumption of turbulent flow, using some form of a pipe flow correlation applied to rocket engines by Bartz.[13] However, use of the correlation sometimes led to an underprediction of the amount of heat transfer in the barrel section, where the boundary layer is in its initial stages of development and an overprediction of heat transfer in the throat region,

where the pressure gradient is large. Integral boundary layer analyses, based on flat plate data with zero pressure gradients, also had problems of accommodating flows in the converging and throat regions, where the pressure gradient is large. There were also questions about determination of the initial conditions and the starting point for the analysis. As a result, rocket heat transfer parameters are usually determined from empirical correlations that are based on data from specific chamber contours, injector designs, and test conditions.

Reference 12 recommends determination of the Stanton number (a dimensionless heat transfer parameter) in the turbulent flow regime, using:

$$St = Cg\ Re^{-0.2}\ Pr^{-0.6} \tag{1}$$

where Cg is an empirically determined correlation coefficient that is a function of position, Re is the Reynolds number, and Pr is the Prandtl number. In the laminar flow regime, reference 12 recommends determination of the Stanton number using:

$$St = 0.318\ Re^{-0.5}\ Pr^{-0.6} \tag{2}$$

where a constant is used as a correlation coefficient. Often, $StPr^{0.6}$, defined as the Stanton-Prandtl grouping number, is used in the above equations as the heat transfer parameter. This defines heat transfer as a function of Reynolds number, which more easily obtainable experimentally than the Prandtl number. The Stanton number can be used to determine the convective heat flux from:

$$\dot{q}'' = St\ \rho\ u\ C_p\ (T_{aw} - T_{wall}). \tag{3}$$

A heat transfer coefficient, h, can be defined as:

$$h = St\ \rho\ u\ C_p. \tag{4}$$

For flows with film cooling, and therefore large temperature differences through the boundary layer, reference 12 recommends calculating the heat flux from the enthalpy difference instead of the temperature difference, to account for the nonconstant specific heat:

$$\dot{q}'' = St\ \rho\ u\ (H_{aw} - H_{wall}). \tag{5}$$

An enthalpy difference heat transfer coefficient, g, can be defined as:

$$g = St\ \rho\ u = {}^{h}/_{C_p}. \tag{6}$$

In rockets where the product of chamber pressure and thrust is under 3100 kN^2/m^2 (10^5 lbf^2/in^2)[12], it has been shown that the boundary layer flow can undergo reverse transition or relaminarization. Relaminarization occurs in the converging section of the rocket, where a turbulent or transitional flow can be suppressed by acceleration effects. Studies have indicated that large convergence angles, large contraction ratios, and small throat radii of curvature promote relaminarization.[12] Empirically established criteria for relaminarization in rockets are given in references 12 and 14. The throat Reynolds number regimes of laminar, transition, and turbulent flow in rockets are shown in figure 1.

Empirical heat transfer correlations based on heated air and rocket data for a range of contraction ratios (2.83 to 19), contraction cone half-angles (30° to 60°), and throat diameters (3.81 to 12.7 cm (1.5 to 5.0 in)), are given in reference 15. These correlations were corrections to the fully turbulent pipe flow equation for low Reynolds number, transitional Reynolds number, and high Reynolds number flow regimes. The equations calculated a Stanton Prandtl grouping number as a function of the chamber geometry and throat Reynolds number, for the converging section, throat, and diverging section of the rocket.

Another empirical model for estimating combustion heat flux, along with performance and stability in gaseous hydrogen/gaseous oxygen rockets is given in reference 16. This model was based on 405 cold flow and hot fire tests with six injector types, for chamber pressures ranging from 690 kPa (100 psia) to 3.45 MPa (500 psia) and mixture ratios from 1 to 8. An analytical model was also developed in the same program for estimates of heat flux outside the empirical envelope.

A priori prediction of the amount of film cooling required in small rockets has been lacking. The amount of mixing and reactions between fuel film and oxidizer-rich core flows has proven to be a difficult parameter to accurately determine from laboratory test data or global rocket parameters. Liquid film cooling flows add further complexity, since they will vaporize and decompose at some point downstream in the chamber. As a result, there has been difficulty in predicting the local flowfield parameters at the chamber wall for flows with film cooling, which adds significant uncertainty in predicting heat transfer.

A heat transfer model accounting for gas film cooling (known as HOCOOL) was developed[17], anchored in testing with hydrogen/oxygen propellants and hydrogen, helium, and nitrogen film cooling at 2.07 MPa (300 psia) chamber pressure. The model assumed two flow streams, a core flow, and a mixing layer, where a percentage of the core flow is considered to be entrained in the film flow. An empirically determined entrainment fraction was used to specify the amount of core flow gases mixed into the film coolant layer. The entrainment fraction was to account for flow turning, acceleration, coolant injection configuration and core injector effects, all of which can significantly affect the heat transfer.

A finite difference film cooling model for a small, regeneratively-cooled, gaseous hydrogen/gaseous oxygen thruster was recently developed.[18] The model divided the rocket into four different regions, a central core flow, wall film coolant flow, wall heat conduction, and regenerative coolant flow. A reacting turbulence model was used to calculate the mixing between the wall film flow and the central core flow. Reasonable agreement between analytical and experimental data was found, but the model has yet to be applied to different injector types or other propellant combinations. Parametric analyses with the code indicated that the film cooling was most efficient when the ratio of film velocity to core velocity was set to one, as this reduced the amount of mixing between the film and core flows. This velocity ratio was determined in large part by the percentage of fuel used for film cooling and the fuel inlet temperature. The initially ambient temperature hydrogen from the regenerative cooling channels and the resulting reduced coolant velocity was thought to be responsible for severe chamber temperature spikes that were sometimes experienced during startup transients of the thruster.

Calorimetry is often used to determine the local heat flux in rockets.[19,20] This method usually uses a series of water-cooled rings along the length of the rocket to determine the one-dimensional heat transfer from the rise in temperature of the water and the water flowrate. Another approach to heat flux determination is the use of an instrumented, thin-walled rocket to acquire time-dependent temperature data and the one-dimensional version of heat conduction equation to solve for heat flux.[20,21] A methodology similar to the one used in this study was performed to determine the local heat transfer coefficient on gas turbine blades.[22] The surface of the turbine blade was instrumented with thermocouples to give the boundary conditions for a numerical solution of the two-dimensional heat conduction equation. Given the normal temperature gradient from the solution of the heat conduction equation, the local heat transfer coefficient could be determined at any point along the blade.

Though the above survey was not comprehensive, it did point to the fact that many of the correlations developed for rocket heat transfer were based on higher Reynolds numbers and chamber pressures than usually encountered in low thrust rockets. Care must be taken in extrapolating these empirical correlations (including the laminar flow correlations) to smaller Reynolds number rockets, as the fundamental nature of the flowfields may differ from the regime for which the correlations were established.

Test Hardware

Injector

The injector used for this study, which had been used in previous small rocket flowfield studies[6,8,10,11,18,23], was fabricated by Gencorp Aerojet Propulsion Division[24] under contract to NASA Lewis Research Center. The injector was originally fabricated for use in a regeneratively-cooled, gaseous hydrogen/gaseous oxygen thruster as part of a Space Station Freedom propulsion technology program. The

design point for this thruster was 517 kPa (75 psia) chamber pressure, 8:1 oxidizer-to-fuel mixture ratio, and 60 percent fuel film cooling. The injector components are shown in figure 2 and a schematic of the injector/chamber assembly is shown in figure 3. A platelet stack injector with spark ignition used a slotted chamber sleeve insert that fit against the injector and extended 2.54 cm (1.00 in) into the chamber. Static pressure taps in the injector measured chamber, hydrogen injection and oxygen injection pressures.

In injector operation, all of the oxygen was radially injected from the platelet stack, upstream of the spark plug tip. The hydrogen entered a manifold, where the flow was divided between the injector and the sleeve insert. The hydrogen diverted into the platelet stack was radially injected just downstream of the spark plug tip, where it mixed with the spark-excited oxygen and ignited. The hydrogen diverted to the sleeve flowed down the axially milled slots in the sleeve for injection into the chamber for film cooling. The dimensions of the slotted flow splitting washer controlled the percentage of hydrogen that was diverted for film cooling. This injector configuration has been used extensively for small rocket flowfield studies because of the sleeve insert feature. The exit of the sleeve was essentially a single element, coaxial injector, composed of a core flow of hydrogen/oxygen combustion products and a surrounding, coannular flow of pure hydrogen. Starting numerical calculations at the sleeve exit greatly simplified the injector modeling that had to be done in developing flowfield codes.[9,10,11]

Chamber

A thick-walled, water-cooled chamber was used in this study, shown in figures 3 and 4. The chamber was fabricated from oxygen-free, high-conductivity (OFHC) copper. The chamber was designed to match the axisymmetric contour of the regeneratively-cooled thruster for which the injector was originally designed, except that the nozzle was cut off at an 1.85 area ratio. The chamber had a diameter of 2.54 cm (1.00 in) in the barrel section, a throat diameter of 1.28 cm (0.503 in), a contraction ratio of 3.96, and a wall thickness of 1.27 cm (0.50 in). Taking the sleeve exit as the start of the chamber, the characteristic chamber length (L*) was 17.2 cm (6.76 in). An OFHC copper housing was welded onto the chamber to provide an annulus for water cooling along the outer wall. The water flowrate in the annulus was on the order of 1.14 lpm (0.3 gpm).

The locations of the thermocouples in the chamber are shown in figure 5. Chromel-alumel, grounded junction thermocouples were used, which were assumed to have a measurement error of +/- 1 °C (2 °F). Two rows of seven thermocouples were embedded in the chamber, nominally 0.159 cm (0.0625 in) away from the inner wall. The inner wall thermocouples were bottomed out in a 0.318 cm (0.125 in) diameter hole that tapers to 0.07938 cm (0.03125 in) at the bottom, insuring good thermal contact with the chamber. Two rows of four thermocouples were attached on the outer wall of the chamber. Each outer wall thermocouple was located at the same axial position as an inner wall thermocouple and approximately ten degrees circumferentially from the inner wall thermocouple row. Along the same rows, a thermocouple was embedded in the front end of the chamber, at the same radial position as the outer wall thermocouples. Thermocouples were also embedded on the exit face, halfway down from the outer diameter and at the same circumferential position as the inner wall thermocouple rows.

Testing

Facility

Testing of the rocket was conducted at NASA Lewis Research Center's low thrust propulsion test facility.[25] The facility was designed for research of low thrust rockets, operating on gaseous hydrogen/gaseous oxygen propellants, at thrust levels from 22 to 220 N (5 to 50 lbf), in long duration steady state or cyclic testing. The rocket was mounted in a 0.91-meter (3-foot), cylindrical test tank with viewports for optical access. A two-stage air ejector system maintained a 1.4 kPa (0.2 psia) pressure in the tank, equivalent to an altitude of 36.6 km. The rocket axis was oriented horizontally in the thrust stand and was mounted on flexible plates to insure freedom of movement along the thrust axis. The rocket was fired into a water-cooled diffuser, where the exhaust was cooled by water spray, prior to entering the air ejectors and venting through mufflers. All data were recorded on a PC-based data acquisition system and performance parameters were calculated in real time, during testing. Hydrogen and oxygen mass flowrates were calculated using the measured inlet pressures, the measured inlet temperatures, and the discharge coefficients of critical flow venturis with corrections for real gas effects.[26] A more detailed description of the test facility is available in reference 25.

Test Program

Testing consisted of 30-second, steady-state tests using the flow splitting washer calibrated to provided 60.9 percent fuel film cooling. Tests were performed for a range of mixture ratios (3.41 to 8.36) with chamber pressures at 414 kPa (60 psia) +/- 14 kPa (2 psia). The mixture ratios in the core flow (which are taken as the overall mixture ratio divided by one minus the fraction of fuel film cooling) were all above stoichiometric, ranging from 8.72 to 21.4. Both outer wall and inner wall thermocouples typically reached steady state within 10 seconds of the start of the test. All of the data used in this study were taken from the last frame of data, at approximately 30 seconds into the test, to insure that only steady-state temperature data were used. Multiple tests were performed at each mixture ratio to insure repeatability of the data.

Measurement Uncertainty

The measurement uncertainties of the mass flowrates and mixture ratio were determined using the JANNAF recommended procedure.[27] With each measured quantity (temperature, pressure), there is a random or precision error and a bias error associated with the calibrations of the measuring instrument and with the data acquisition of the measurement. The uncertainty of the parameters calculated from the measured quantities are a combination of the precision and bias errors of the measured quantities, propagated to the calculated values. In this study, the temperature and pressure measurements were assumed to have zero bias errors. The largest contributors to the errors of the parameters were the venturi inlet pressure and venturi discharge coefficient calibration errors used in the mass flowrate calculations. The measurement uncertainties for this test series were:

Chamber Pressure:	+/- 0.5 %
Hydrogen Mass Flowrate:	+/- 1.2 to 1.7 %
Oxygen Mass Flowrate:	+/- 2.4 to 3.9 %
Total Mass Flowrate:	+/- 1.2 to 1.5 %
Mixture Ratio:	+/- 3.0 to 4.1 %

Finite Element Model

MSC/NASTRAN

MSC/NASTRAN[28] is a general purpose, finite element analysis computer program for solving a variety of engineering problems including static and dynamic structural analysis, heat transfer, acoustics, and electromagnetism. MSC/NASTRAN is a proprietary version of NASTRAN®, the NASA structural analysis program, marketed by the MacNeal-Schwendler Corporation. In this study, MSC/NASTRAN was used for the thermal analysis[29] of a thick-walled rocket chamber. In the program, the rocket chamber was subdivided into small regions or elements, which were connected together by a series of grid points. Specifying either temperatures or no heat input (adiabatic) for the outer grid points as boundary conditions, the temperatures of the interior grid points were determined using finite element analysis and the resulting temperature gradients and heat fluxes (given a thermal conductivity) for the elements were calculated.

Version 67 (September 10, 1991) of MSC/NASTRAN was used for this study (implementing the solution 61 algorithm) and was run on the Cray X-MP system. The input was set up as a linear, steady state heat transfer problem in axisymmetric coordinates. (Transient and nonlinear heat flux problems can also be determined, if desired, using the appropriate modules in MSC/NASTRAN). OFHC copper is composed of 99 percent copper, so a thermal conductivity of 393 W/(m - °C) (0.00525 Btu/(sec-in-°F)) was used in the program, the thermal conductivity of pure copper at 149 °C (300 °F). This was assumed to be a reasonable value, as the thermal conductivity of pure copper varies only by 1.5 percent from 93 °C (200 °F) to 247 °C (400 °F).[30]

The chamber was broken down to a grid as shown in figure 6. In the axial direction, 99 grid points were used, while 5 grid points were used in the radial direction, creating 495 grid points and 392 elements. The axisymmetric trapezoidal ring elements of MSC/NASTRAN were used in formulating all of the elements. Defining Z as the axial direction and R as the radial direction, from Z = 0.00 cm to 2.54 cm, the elements were 0.3175 cm by 0.3175 cm (0.125 in by 0.125 in). Beginning at the sleeve exit (Z = 2.54 cm) to the nozzle exit (Z = 8.08 cm), the elements were generally 0.0635 cm (0.025 in) in the axial direction by 0.3175 cm (0.125 in) in the radial direction.

Boundary Conditions

The boundary conditions for the finite element model were implemented by either specifying a temperature or a heat load for each outer grid point. The boundary condition assumptions are shown in figure 7. On the face bordering the hydrogen inlet manifold (Z = 0.00 cm, R = 1.27 cm to R = 2.54 cm), an adiabatic wall was specified by imposing a heat load equal to zero on each of the grid points. Considering that this face only saw low speed, ambient temperature gaseous hydrogen, the adiabatic wall assumption was felt to be reasonable. The exit face (Z = 8.08 cm) was assumed to be an isothermal surface. The five exit face grid points, then, were given the same temperature as the thermocouple located halfway down the exit face. Temperatures were specified for the inner and outer wall grid points using interpolation and extrapolation of the thermocouple data, as given in Table 1.

Grid points with thermocouple measurements or interpolated thermocouple measurements provided a relatively high measure of confidence as boundary conditions. The most questionably defined boundary conditions were the extrapolated temperatures at the grid points downstream of the throat and at the head end along the inner wall, and the isothermal assumptions on the exit face. Running MSC/NASTRAN with varying temperature at these grid points showed that most of the changes in radial heat flux magnitude occurred at the ends and that the fundamental heat flux profiles between the sleeve exit and throat had not changed. This study, then, concerned itself with the heat flux profiles from the sleeve exit (Z = 2.54 cm) to the throat (Z = 7.62 cm), as this section appeared to be insensitive to boundary conditions defined outside the coverage of the thermocouples.

During testing the exit face received heat input from recirculation of the plume, due to the short area ratio (1.85:1) of the nozzle used and problems with the facility diffuser capturing the entire plume. Undoubtedly, this heating of the exit face was uneven, undercutting the isothermal assumption. MSC/NASTRAN was run with a 1.06 kW (1.0 Btu/sec) heat load imposed on the exit face grid points, in order to assess the effect of the plume recirculation. Radial heat flux increased from the original values downstream of the throat, as would be expected, but the heat flux profiles and magnitudes did not change significantly upstream of the throat. The plume recirculation, then, did not appear to affect the heat flux results between the sleeve exit and throat.

With the thermocouples located 0.159 centimeters (0.0625 inches) away from the inner wall, there was concern whether they would accurately reflect the inner wall temperature profile. The main reason for not placing the thermocouples closer to the inner wall was the possibility of distorting the inner wall contour while drilling the thermocouples holes. The program was run initially with the embedded thermocouples representing the inner wall. Some elements in the higher mixture ratio runs had calculated large radial temperature gradients, warranting iteration on the inner wall temperature profile. Iteration was performed by extrapolating the temperature profile defined by the thermocouple data to the inner wall, using the radial temperature gradients calculated in the initial MSC/NASTRAN runs. The program was rerun using the extrapolated inner wall temperature profile. Although the calculated heat fluxes generally increased by 15 to 20 percent, they were still on the same order of magnitude and, more importantly, still exhibited the same heat flux profiles over the mixture ratio range as the initial run. Since the one-dimensional extrapolation of inner wall temperature was not accurate in this two-dimensional problem and since the heat flux profiles rather than the absolute values were the main focus of this study, the initial MSC/NASTRAN runs were used. Chambers with thermocouples closer to or flush with the inner wall would be preferred to better represent the inner wall temperature boundary conditions.

Another concern was whether there would be sufficient coverage of thermocouples to accurately detect changes in the heat flux as a function of axial position. Restricting the number of thermocouples that had to be installed better facilitated fabrication of the chamber. However, more thermocouples would have provided better definition of the boundary conditions (using more measured instead of interpolated temperatures) and resulted in better resolution of the heat flux profile. As discussed below, there was a concern that the shape of the heat flux profiles would be overly sensitive to thermocouple location and the curve fit used for interpolating between thermocouples.

Results and Discussion

Finite Element Program Output

The inner wall and outer wall thermocouple data for each mixture ratio (MR) case used in this study are

shown in figures 8 and 9, respectively. Using the thermocouple data to define the boundary conditions, MSC/NASTRAN was run to calculate the radial and axial heat fluxes for each element. The normal heat flux for each element was then found as the dot product of the resultant heat flux vector and the normal vector, that is:

$$|\dot{q}_n''| = \vec{q}_T \bullet \vec{n} = \dot{q}_R'' \cos\theta + \dot{q}_Z'' \sin\theta \qquad (7)$$

where theta is the angle normal to the surface, measured from the radial axis. In the barrel section theta was equal to zero, so the normal heat flux there was equal to the radial heat flux.

The inner wall, normal heat flux calculated from the thermocouple data is plotted as a scatter graph in figure 10, as a function of axial position. In the barrel section, the MR = 3.41 and MR = 4.00 cases gradually increased in heat flux to the beginning of the converging section. For the MR = 4.97 and higher mixture ratio cases, there was a sharp increase in the normal heat flux profile, from the sleeve exit to the middle of the barrel section, where a local maximum occurred. The normal heat flux curve then declined and generally leveled off to the beginning of the converging section. In the converging section, the shape of the normal heat flux curves were the same for all MR cases, although the magnitudes were larger for the higher mixture ratio cases. The heat flux curves declined to a minimum around Z = 6.50 cm, then increased to the maximum normal heat flux before decreasing to the throat.

The normal heat flux maximums, both in the barrel and converging sections, occurred around thermocouple locations. A grid point using a thermocouple measurement represented the extrema of temperature data, however, the adjoining grid points used interpolated values for temperatures. Since the temperature gradients through elements rather than from grid point to grid point were calculated, the location and magnitude of heat flux peaks would be sensitive, to some degree, to the interpolated grid point temperatures. The finite element analyses were performed with both linear and second-order polynomial curve fits for the interpolation of the thermocouple data in the regions corresponding to the heat flux maximums. Though the polynomial curve fits resulted in a smoother peak, the fundamental shape of the heat flux profiles did not change. Polynomial curve fits of thermcouple data were used in the regions corresponding to the heat flux maximums.

The maximum normal heat flux for all MR cases occurred at Z = 6.86 cm to 7.11 cm, ranging from 1.32 MW/m^2 (0.804 Btu/sec-in^2) for the MR = 3.41 case to 3.18 MW/m^2 (1.94 Btu/sec-in^2) for the MR = 8.36 case. For the higher MR cases, the local heat flux maximums in the barrel section occurred between Z = 4.00 cm to 4.50 cm. The MR = 4.97 case had the highest heat flux value there, 3.07 MW/m^2 (1.87 Btu/sec-in^2). In the same region, the heat fluxes ranged from 2.89 MW/m^2 (1.76 Btu/sec-in^2) for the MR = 5.84 case down to 2.26 MW/m^2 (1.38 Btu/sec-in^2) for the MR = 8.36 case. Thermal contour plots for the MR cases in this study were also generated by the MSC/NASTRAN program and are shown in Appendix A.

Flowfield Behavior

Using the measured heat fluxes and equation (5), the enthalpy difference heat transfer coefficient was found and plotted as a function of axial position in figure 11. The chemical equilibrium composition (CEC) computer code[31,32] was used to calculate the wall enthalpy from the measured wall temperature and the flow properties at the reference enthalpy[30] (see Appendix B for details about the flow properties calculations). As expected, the heat transfer coefficient profiles followed the same trend as the heat flux profiles.

In the converging section, the changes in the normal heat flux profiles corresponded with changes in the chamber contour. Figure 12 shows the angle normal to the inner wall (measured from the radial axis) in the converging section plotted as a function of axial position. The normal angle steadily increased from the beginning of the converging section to about Z = 6.50 cm, where the chamber contour went from a curved, convex surface to a straight line, conical section. It is at this point where the normal heat flux minimums occurred. In the straight line section, where the normal angle was constant, the normal heat fluxes steadily increased to their maximum values. As the contour changed from a straight line, conical surface to a curved, concave surface (around Z = 6.90 cm), the normal heat fluxes began to decrease.

In the barrel section, there was a difference between the MR = 3.41 and 4.00 cases and the higher mixture ratio cases, for which there were local normal heat flux maximums approximately 1.5 to 2.0 cm downstream of the sleeve exit. These local maximums would appear to be indicators of some type of flowfield

phenomenon triggered at higher mixture ratios. The heat flux maximums would be consistent with transitioning from laminar flow to turbulent flow. Figure 13 shows Reynolds number plotted as a function of axial position, where viscosity was evaluated at the reference enthalpy. The MR = 3.41 and 4.00 cases had larger Reynolds numbers than the higher MR cases, which were generally grouped together. The mass flowrate and the viscosity both increased monotonically with increasing mixture ratio. For all the MR cases, the barrel section Reynolds numbers were under 25,000 and the throat Reynolds number were under 45,000, which is well within the laminar flow regime in figure 1. This indicated that the flow in this small rocket was completely laminar and that the local heat flux maximums in the barrel section were not an indication of a transition from laminar flow to turbulent flow.

Another explanation for the local heat flux maximums in the higher MR cases is the reduction or breakdown of the wall film cooling layer. Increased mixing of the oxidizer-rich core gases into the shear layer, with the resulting increase in shear layer combustion could have been responsible for the reduction or breakdown of the film cooling layer. It has been speculated[11] that an unsteady vortex phenomenon exists in this type of flowfield, promoting mixing between the film and core flows. It is difficult, however, to confirm the existence of this unsteady phenomenon without local flowfield measurements.

The increase in shear layer combustion may be more directly related to the amount of oxygen available in the core flow. As mixture ratio increased, the amount of hydrogen available for film cooling decreased and the amount of oxygen in the core increased. The heat flux profiles would seem to indicate that the lower MR cases had little or no excess oxygen in the core, while the higher MR cases had oxygen available to react with the film. Figure 14 shows the core flow mixture ratio as it varied with overall mixture ratio. All of the MR cases had core mixture ratios above stoichiometric, though the actual amount of oxygen available would be dependent on the core combustion efficiency, that is, the combustion efficiency within the chamber sleeve insert. The core combustion efficiency and how it varied with mixture ratio were not measured in this study.

Comparison to Laminar Pipe Flow Correlation

The MSC/NASTRAN generated results were compared to the laminar pipe flow correlation (equation (2)), with Stanton-Prandtl grouping number used as the heat transfer parameter. The measured Stanton-Prandtl grouping numbers were determined using the MSC/NASTRAN calculated normal heat fluxes and flow properties evaluated at the reference enthalpy. A representative low mixture ratio case (MR = 3.41) and high mixture ratio case (MR = 5.84) are shown in figure 15, with the pipe correlation shown as a line and the measured values shown as a symbol. The laminar pipe flow correlation overpredicted the heat transfer for all MR cases in the converging section, with the correlation two to four times greater than the measured values at the throat. Also, the laminar pipe flow correlations were significantly higher than the measured values at the sleeve exit for all MR cases. In the barrel section, however, the difference between the lower and higher mixture ratio cases were highlighted once again. For the low mixture ratio cases, the laminar pipe flow correlations were two to three times higher than the measured values. However, for mixture ratios above 5, the measured Stanton-Prandtl values were significantly closer to the laminar pipe flow correlations (within five to fourty percent) and in some instances higher than the correlations. The region where there was better agreement between measured and correlation values corresponded with the local heat flux maximums, though the reasons for this are not clear. It is interesting to note, however, this occurred where the effects of film cooling on heat transfer were probably the least impactive.

Summary

To better understand the mixing and heat transfer phenomena in small rockets, an effort has been undertaken to gather local and global data on small rocket flowfields and to apply numerical models developed in the aeronautical community to rocket flowfield modeling. In this study, normal heat flux profiles in a small gaseous hydrogen/gaseous oxygen rocket were determined as a diagnostic of the flowfield behavior. A thick-walled, water-cooled OFHC copper rocket chamber, instrumented with thermocouples, was used to gather steady-state, inner and outer wall temperature profiles over a mixture ratio range from 3.41 to 8.36, at sixty percent fuel film cooling. These temperature profiles were used as boundary conditions in a finite element model of the rocket chamber wall. A finite element program, MSC/NASTRAN, was used to calculate the radial and axial heat fluxes for each element in the rocket chamber model. Normal heat flux profiles were then calculated from the radial and axial heat flux profiles and chamber contour.

The normal heat fluxes determined for this study were on the order of 1.0 to 3.0 MW/m^2 (0.6 to 1.8 Btu/sec-in^2). In the barrel section of the chamber there was a smooth rise in normal heat flux to the converging section for mixture ratios of 4 and less. However, there were sharp local heat flux maximums in the barrel section for mixture ratios of 5 and above. These local maximums would seem to have indicated a reduction or breakdown of the fuel film cooling layer, possibly due to increased mixing in the shear layer between the film and core flows. Since the flows were thought to be completely laminar, as the Reynolds numbers were below 50,000 for all the cases in this study, the increased shear layer mixing in the higher mixture ratio cases was not thought to be due to the flow transitioning to turbulent. Rather, the increased shear layer mixing was thought to be due to increased reactions between the hydrogen film and oxidizer-rich core flows. It was difficult to correlate the behavior indicated by the heat flux values with flow parameters without local measurements in the flowfield. The throat heat fluxes determined in this study were found to be two to four times lower compared to the heat transfer values calculated using the established laminar pipe flow correlation. However, there was much better agreement between the measured and correlation values in the barrel section, for the high mixture ratio cases, corresponding to the local heat flux maximums.

With this methodology the heat flux can be determined independent of flowfield property definition (only the thermal conductivity of the test piece is required), an important consideration for small rocket flows. This methodology is useful as a diagnostic of small rocket flowfields by comparing relative heat flux values over varying conditions (mixture ratio, fuel film cooling percentages, etc.), not necessarily for determining absolute heat flux values. For example, because of the cold wall boundary, this methodology is not appropriate for determining heat flux for chambers with a significant amount of radiation cooling. Definition of the boundary conditions was important in the accuracy and resolution of the heat flux profiles generated by the finite element program. The inner wall thermocouples should be close to or flush with the inner wall, to truly reflect the inner wall temperature profile. The installation of more thermocouples down the length of the chamber would give more measured as opposed to interpolated temperature boundary points, which would result in better resolution of the heat flux profiles.

Appendix A: Thermal Contour Plots

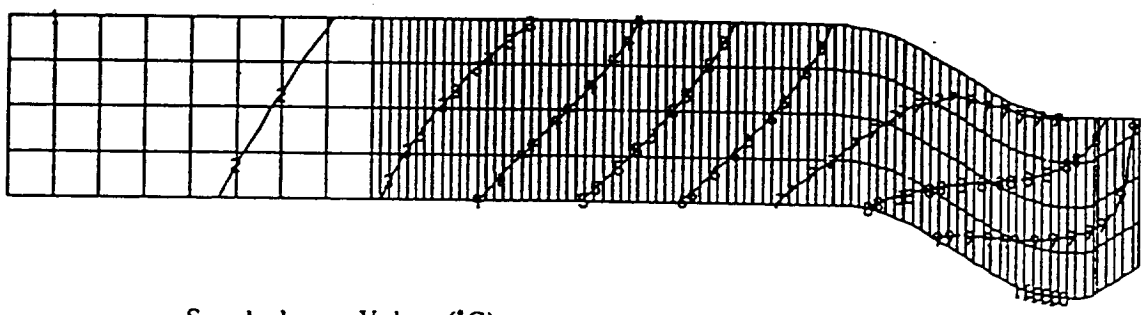

Symbol	Value (°C)
1	28
2	39
3	49
4	61
5	72
6	82
7	93
8	104
9	115
10	126

Thermal Contour for MR = 3.41 Case

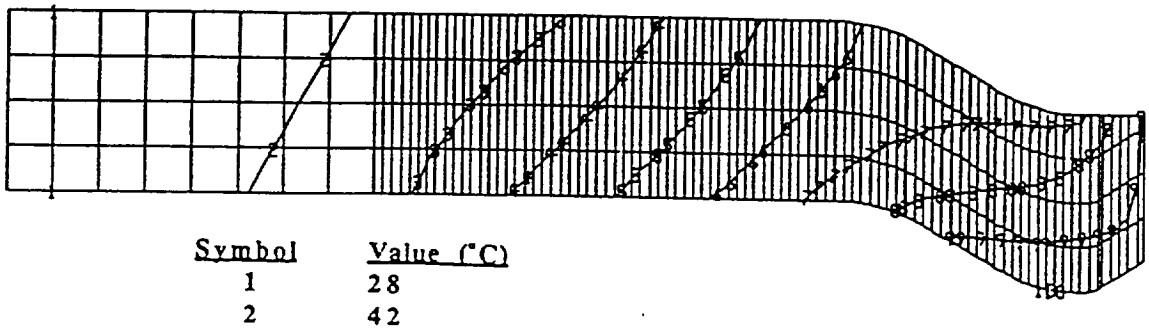

Symbol	Value (°C)
1	28
2	42
3	56
4	69
5	82
6	96
7	109
8	123
9	137
10	150

Thermal Contour for MR = 4.00 Case

Appendix A: Thermal Contour Plots (con't)

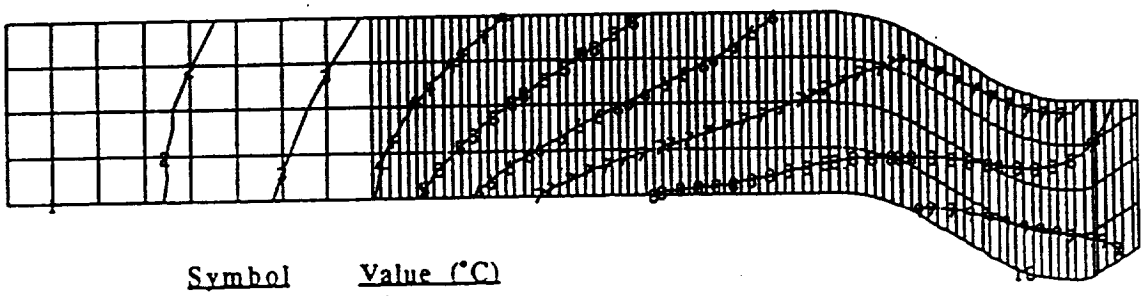

Symbol	Value (°C)
1	31
2	54
3	77
4	101
5	124
6	147
7	171
8	194
9	217
10	241

Thermal Contour for MR = 4.97 Case

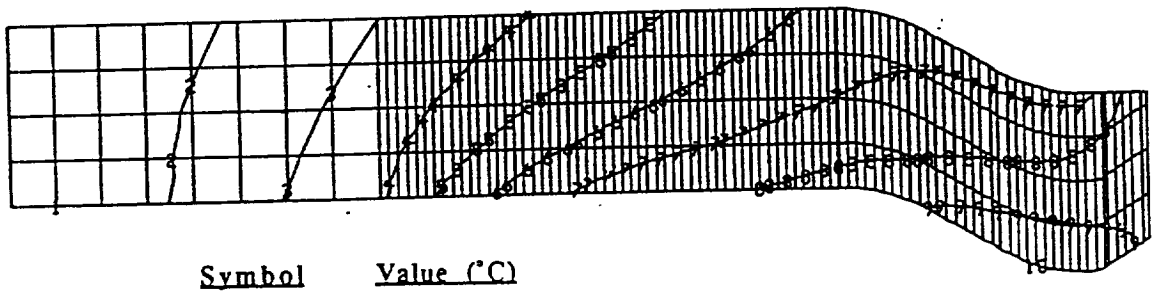

Symbol	Value (°C)
1	31
2	54
3	78
4	101
5	124
6	148
7	172
8	195
9	218
10	242

Thermal Contour for MR = 5.84 Case

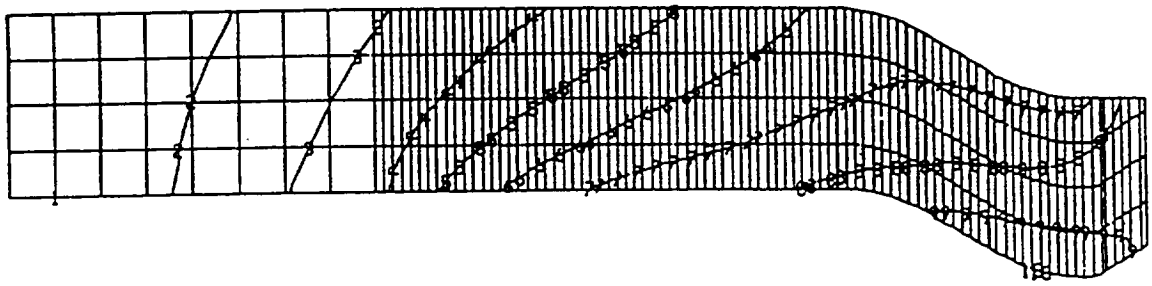

Symbol	Value (°C)
1	32
2	56
3	79
4	102
5	125
6	148
7	172
8	194
9	218
10	241

Thermal Contour for MR = 6.80 Case

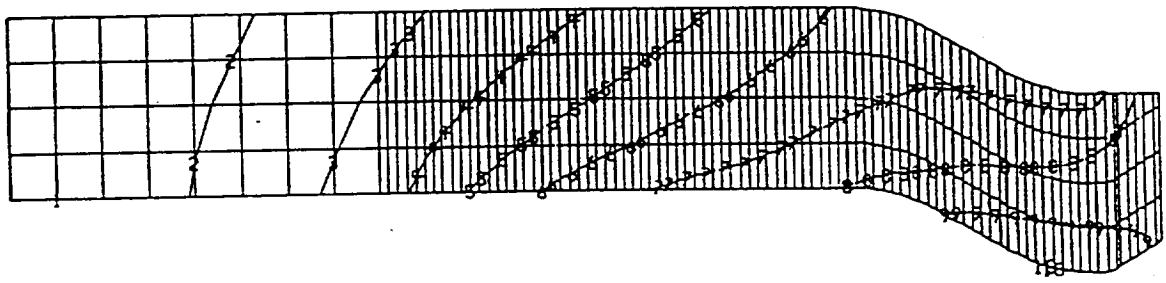

Symbol	Value (°C)
1	33
2	57
3	80
4	103
5	126
6	149
7	173
8	196
9	219
10	242

Thermal Contour for MR = 7.51 Case

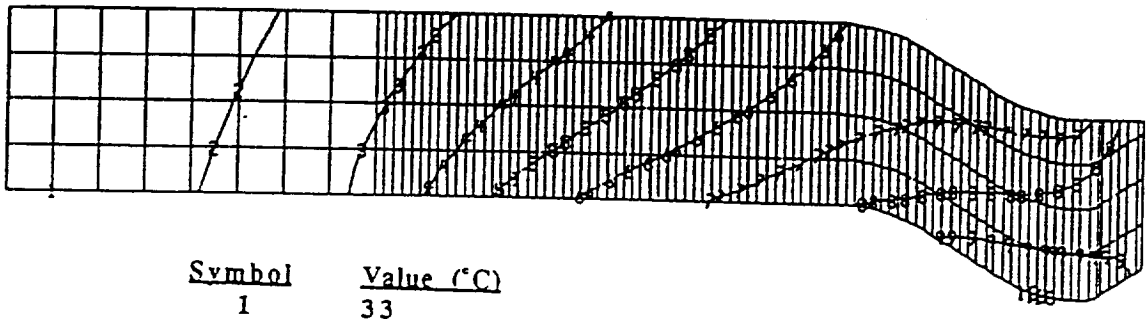

Symbol	Value (°C)
1	33
2	57
3	81
4	104
5	127
6	151
7	174
8	198
9	222
10	245

Thermal Contour for MR = 8.36 Case

Appendix B: Determination of the Gas Flow Properties

The experimental method used in this study to determine heat flux did not require knowledge of the gas flow transport properties or combustion temperature. Only the thermal conductivity of the test piece and the measured wall temperatures were required for the finite element program. However, for the calculation of Reynolds numbers and heat transfer coefficients, the properties of the gas flow and the difference between the wall and adiabatic wall enthalpies were needed. A reference temperature is often used instead of the freestream static temperature to define flow properties in rocket flowfields, in order to account for the variation of properties through the thermal boundary layer. The adiabatic wall temperature or the arithmetic mean of the wall and adiabatic wall temperatures is sometimes used as the reference temperature. For flows with very large temperature differences, such as flows with film cooling, the specific heat cannot be considered constant and the properties should instead be evaluated at a reference enthalpy.[33] Eckert[34] suggested the following expression for reference enthalpy:

$$H_R = H_\infty + 0.5(H_{wall} - H_\infty) + 0.22(H_{aw} - H_\infty) \qquad (8)$$

where H_∞ was the freestream static enthalpy, H_{wall} was the gas flow enthalpy at the wall, and H_{aw} was the adiabatic wall enthalpy given by

$$H_{aw} = H_\infty + r_c(H_{o\infty} - H_\infty) \qquad (9)$$

where $H_{o\infty}$ was the freestream stagnation enthalpy and r_c was the recovery factor, approximated as the square root of the Prandtl number for laminar flow and the cubed root of the Prandtl number for turbulent flow, the Prandtl number evaluated at the reference enthalpy.

In this study the flow properties were evaluated at the reference enthalpy. Using the measured overall mixture ratio and chamber pressure as inputs to the CEC[31,32] code, the freestream static and stagnation enthalpies, as well as the Prandtl number were found. The square root of the Prandtl number was taken as the recovery factor, since laminar flow was indicated. (The turbulent flow recovery factor still yielded Reynolds numbers well into the laminar flow regime). Using the measured wall temperature, overall mixture ratio and chamber pressure, the CEC code was used to find the enthalpy at the wall . The reference enthalpy was then calculated from the above equation and used as input to the CEC code to calculate the flow properties. If the newly calculated Prandtl number did not agree within one percent of the previous value, reference enthalpy was found again using the new recovery factor and input to CEC for another iteration. Typically only one iteration was required.

The possible variation in flow properties is illustrated in figure 16, where Reynolds number calculated by differing estimates of viscosity is plotted against mixture ratio. In this figure, viscosity at the throat was estimated by CEC assuming equilibrium reactions, CEC assuming frozen reactions, Eckert's reference temperature method, and Eckert's reference enthalpy method (the one used in this study).

References

1. Schneider, S.J., "Low Thrust Chemical Rocket Technology", NASA TM-105927, IAF Paper 92-0669, September 1992.

2. Chazen, M.L., et. al., "Space Storable Rocket Technology Program", Final Report - Basic Program, Contract NAS3-26246, TRW Applied Technology Division, NASA CR-189131, May 1992.

3. Reed, B.D. and Schneider, S.J., "Hydrogen/Oxygen Auxiliary Propulsion Technology", NASA TM-105249, AIAA Paper 91-3440, September 1991.

4. Richter, G.P. and Price, H.G., "Proven, Long-Life Hydrogen/Oxygen Thrust Chambers for Space Station Propulsion", NASA TM-88822, 1986 JANNAF Propulsion Meeting, August 1986.

5. Zupanc, F.J. and Weiss, J.M., "Rocket Plume Flowfield Characterization Using Laser Rayleigh Scattering", AIAA Paper 92-3351, July 1992.

6. de Groot, W.A. and Weiss, J.M., "Species and Temperature Measurement in H2/O2 Rocket Flow Fields by Means of Raman Scattering Diagnostics", NASA CR-189217, AIAA Paper 92-3353, July 1992.

7. de Groot, W.A. and Zupanc, F.J., "Laser Rayleigh and Raman Diagnostics for Small Hydrogen/Oxygen Rockets", NASA TM-105999, January 1993.

8. Morren, S. and Myers, R., "A Laboratory Model of a 110 N Thrust, Hydrogen/Oxygen Engine for Combustion and Nozzle Studies", AIAA Paper 93-1825, June 1993.

9. Kim, S.C. and VanOverbeke, T.J., "Calculations of Gaseous Hydrogen/Oxygen Thrusters", AIAA Paper 90-2490, July 1990.

10. Reed, B.D., Penko, P.F., Schneider, S.J., and Kim, S.C., "Experimental and Analytical Comparison of Flowfields in a 110 N (25 lbf) H2/O2 Rocket", NASA TM-105175, AIAA Paper 91-2283, June 1991.

11. Weiss, J.M. and Merkle, C.L., "Numerical Investigation of Reacting Flowfields in Low Thrust Rocket Engine Combustors", AIAA Paper 91-2080, June 1991.

12. "Liquid Rocket Engine Self-Cooled Combustion Chambers", NASA SP-8124, September 1977.

13. Bartz, D.R., "A Simple Equation for Rapid Estimation of Rocket Nozzle Convective Heat Transfer Coefficients", Jet Propulsion, Vol. 27, No. 1, January 1957, pp. 49-51.

14. Smith, T.A., "Boundary Layer Development as a Function of Chamber Pressure in the NASA Lewis 1030:1 Area Ratio Rocket Nozzle", NASA TM-100917, AIAA Paper 88-3301, July 1988.

15. von Glahn, U.H., "Correlation of Gas-Side Heat Transfer For Axisymmetric Rocket Engine Nozzles", NASA TM X-1748, February 1969.

16. Calhoon, D.F., Ito, J.I., and Kors, D.L., "Investigation of Gaseous Propellant Combustion and Associated Injector/Chamber Design Guidelines", Final Report, Contract NAS3-14379, Aerojet Liquid Rocket Company, NASA CR-121234, July 1973.

17. Rousar, D.C. and Ewen, R.L., "Combustion Effects on Film Cooling", Final Report, Contract NAS3-17813, Aerojet Liquid Rocket Company, NASA CR-135052, February 1977.

18. Jeng, S-M and Ippolito, S.A., "Prediction of Fuel Film Cooling", AIAA Paper 90-2511, July 1990.

19. Schoenman, L., "LOX/Propane and LOX/Ethanol Combustion Chamber Heat Transfer", AIAA Paper 87-1875, July 1987.

20. Witte, A.B. and Harper, E.Y., "Experimental Investigation and Empirical Correlation of Local Heat Transfer Rates in Rocket Engine Thrust Chambers", Jet Propulsion Labortory Technical Report 32-244, March 1962.

21. Kacynski, K.J., Pavli, A.J., and Smith, T.A., "Experimental Evaluation of Heat Transfer on a 1030:1 Area Ratio Rocket Nozzle", NASA TP-2726, August 1987.

22. Turner, A.B., "Local Heat Transfer Measurements on a Gas Turbine Blade", Journal of Mechanical Engineering Science, Vol. 13, No. 1, June 1971.

23. Arrington, L.A. and Reed, B.D., "Performance Comparison of Axisymmetric and Three-Dimensional Hydrogen Film Coolant Injection in a 110 N Hydrogen/Oxygen Rocket", NASA TM-105967, AIAA Paper 92-3390, July 1992.

24. Robinson, P.J., "Space Station Auxiliary Thrust Chamber Technology", Final Report, Contract NAS3-24398, GenCorp Aerojet Propulsion Division, NASA CR-185296, July 1990.

25. Arrington, L.A. and Schneider, S.J., "Low Thrust Rocket Test Facility", NASA TM-103206, AIAA Paper 90-2503, July 1990.

26. "Fluid Meters: Their Theory and Application", American Society of Mechanical Engineers, 1971.

27. "Handbook for Estimating the Uncertainty in Measurements Made with Liquid Propellant Rocket Engine Systems", Chemical Propulsion Information Agency Document Number 180, April 1969.

28. "MSC/NASTRAN User's Manual, Version 67", MacNeal-Schwendler Corporaton, 1992.

29. "MSC/NASTRAN Handbook for Thermal Analysis", MacNeal-Schwendler Corporation, November 1986.

30. Incropera, F.P. and DeWitt, D.P., "Fundamentals of Heat and Mass Transfer", John Wiley & Sons, Inc., 2nd Edition, 1985.

31. Gordon, S. and McBride, B., "Computer Program for Calculation of Complex Chemical Equilibrium Composition, Rocket Performance, Incident and Reflected Shocks, and Chapman-Joguet Detonations", NASA SP-273, March 1976.

32. Gordon, S., McBride, B., and Zeleznik, F., "Computer Program for Calculation of Complex Chemical Equilibrium Compositions and Applications: Supplement I - Transport Properties", NASA TM-86885, October, 1984.

33. Kays. W.M. and Crawford, M.E., "Convective Heat and Mass Transfer", McGraw-Hill Book Company, 2nd Edition (reissue), 1987.

34. Eckert, E.R.G., "Engineering Relations for Heat Transfer from Rapidly Accelerating Flow of Rocket Turbulent Boundary Layer Flow Over Surfaces with Constant Pressure and Temperature", Trans. ASME, Vol. 78, 1956, pp.1273-1283.

Table 1: Curve Fit of Thermocouple Data

Inner Wall: Z, Axial Distance (cm)	Curve Fit
0.318 to 1.27	Extrapolation of the Z = 1.27 cm to 2.54 cm line fit
1.27 to 2.54 (sleeve exit)	Straight line fit of thermocouple data
2.54 to 5.08	Second order polynomial curve fit of thermocouple data
5.08 to 6.35	Straight line fit of thermocouple data
6.35 to 7.62 (throat)	Second order polynomial curve fit of thermocouple data
7.62 to 8.08 (nozzle exit)	Straight line fit of the thermocouple at Z = 7.62 cm and the assumed exit face temperature

Outer Wall: Z, Axial Distance (cm)	Curve Fit
0.318 to 1.25	Straight line fit of thermocouple data
1.25 to 3.81	Straight line fit of thermocouple data
3.81 to 6.35	Straight line fit of thermocouple data
6.35 to 7.62 (throat)	Straight line fit of thermocouple data
7.62 to 8.08 (nozzle exit)	Straight line fit of the thermocouple at Z = 7.62 cm and the assumed exit face temperature

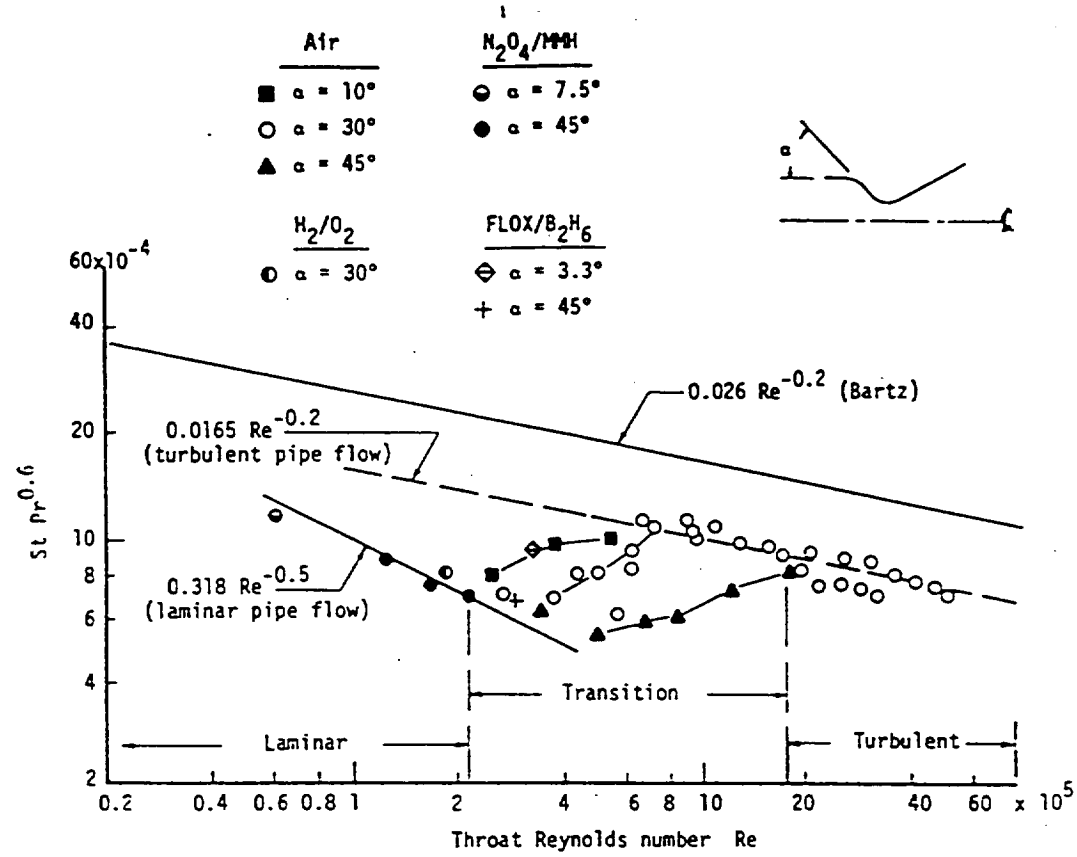

Figure 1: Heat Transfer vs. Throat Reynolds Number[12]

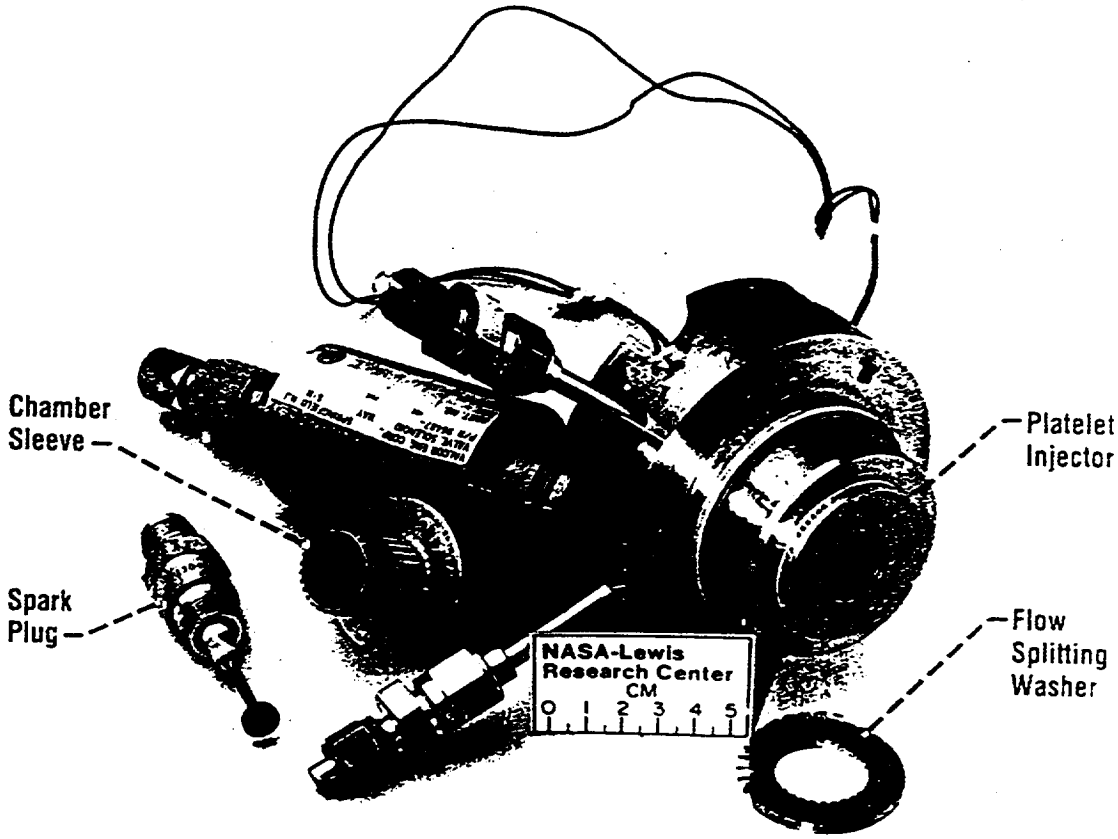

Figure 2: Injector Components

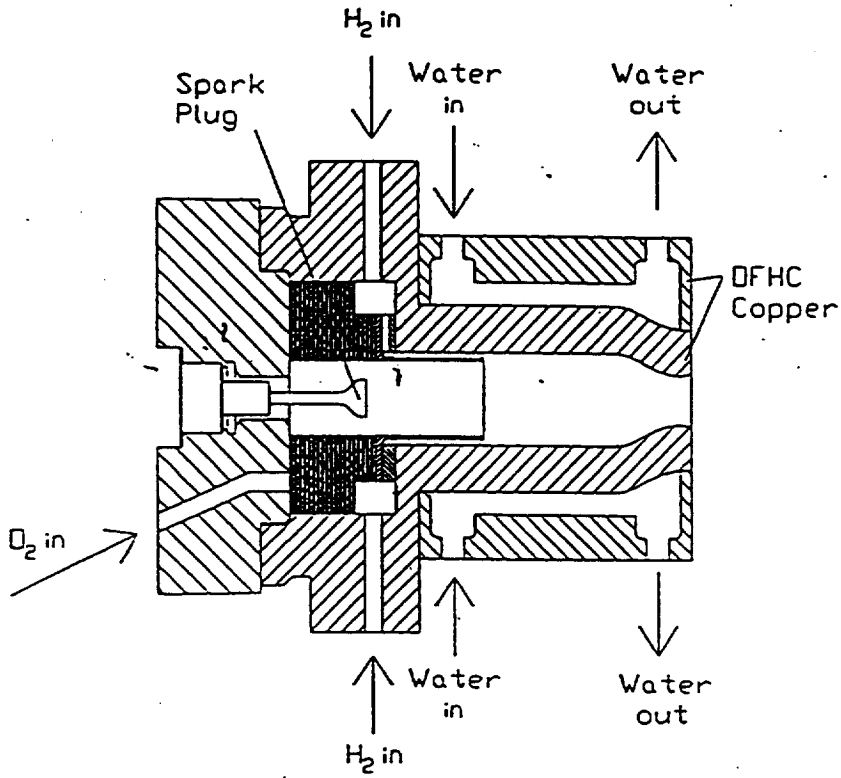

Figure 3: Heat Flux Chamber Schematic

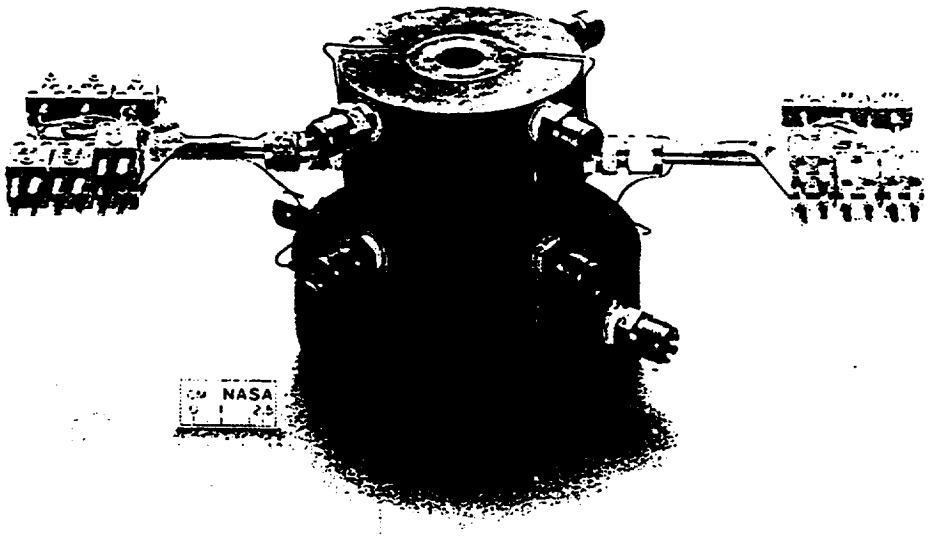

Figure 4: Heat Flux Chamber

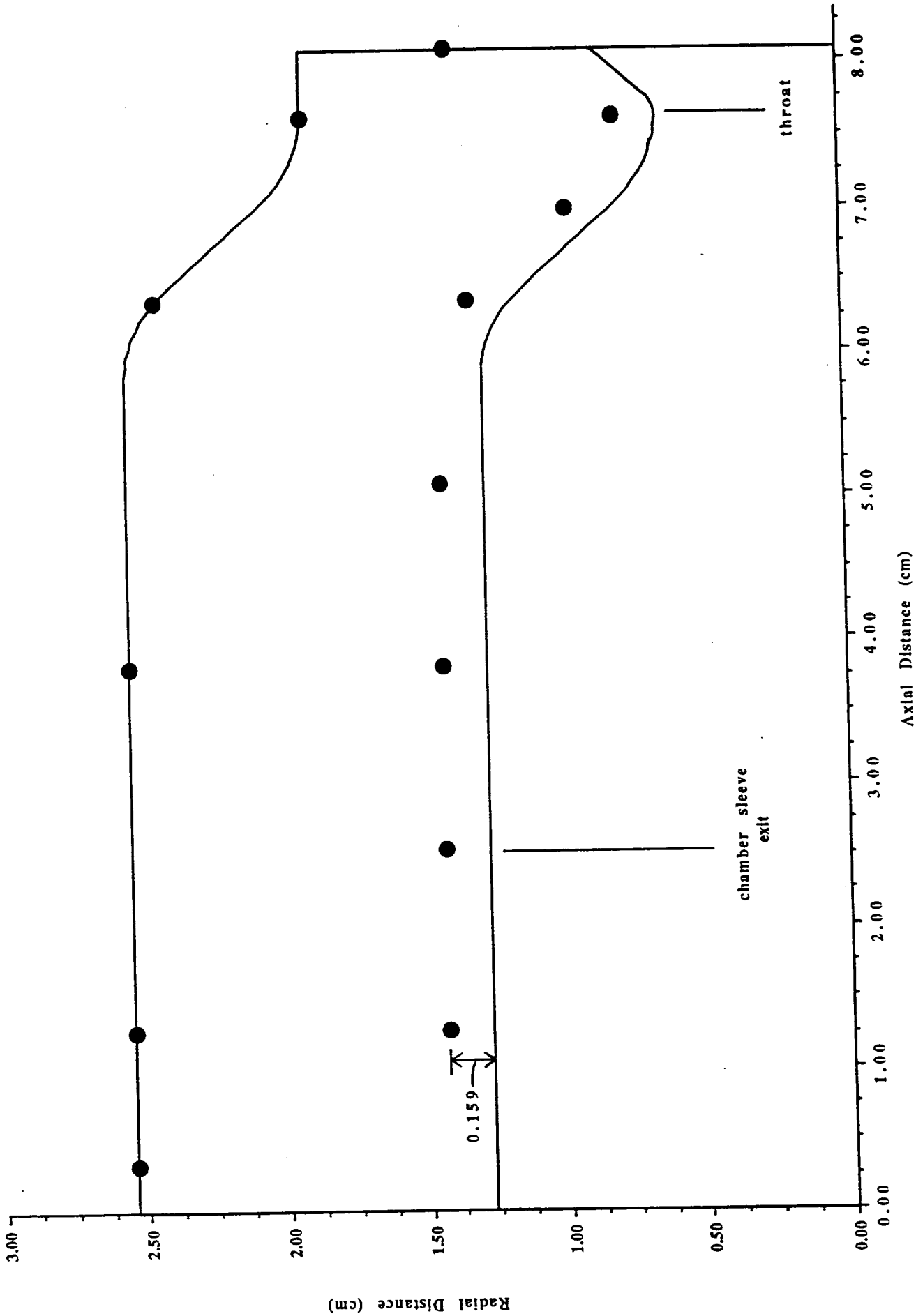

Figure 5: Thermocouple Locations in Heat Flux Chamber
• Denotes Thermocouple

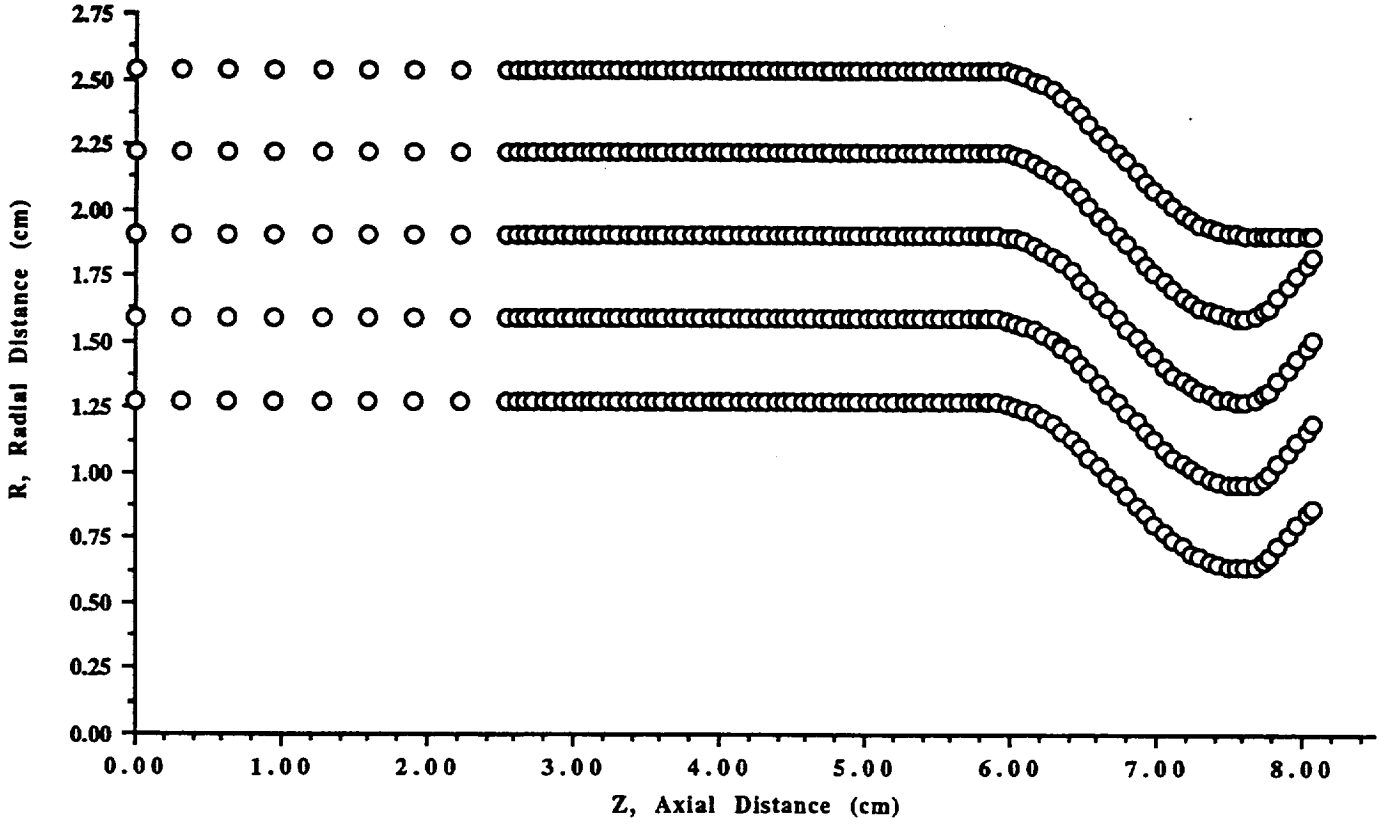

Figure 6: Grid Point Definition for Finite Element Model

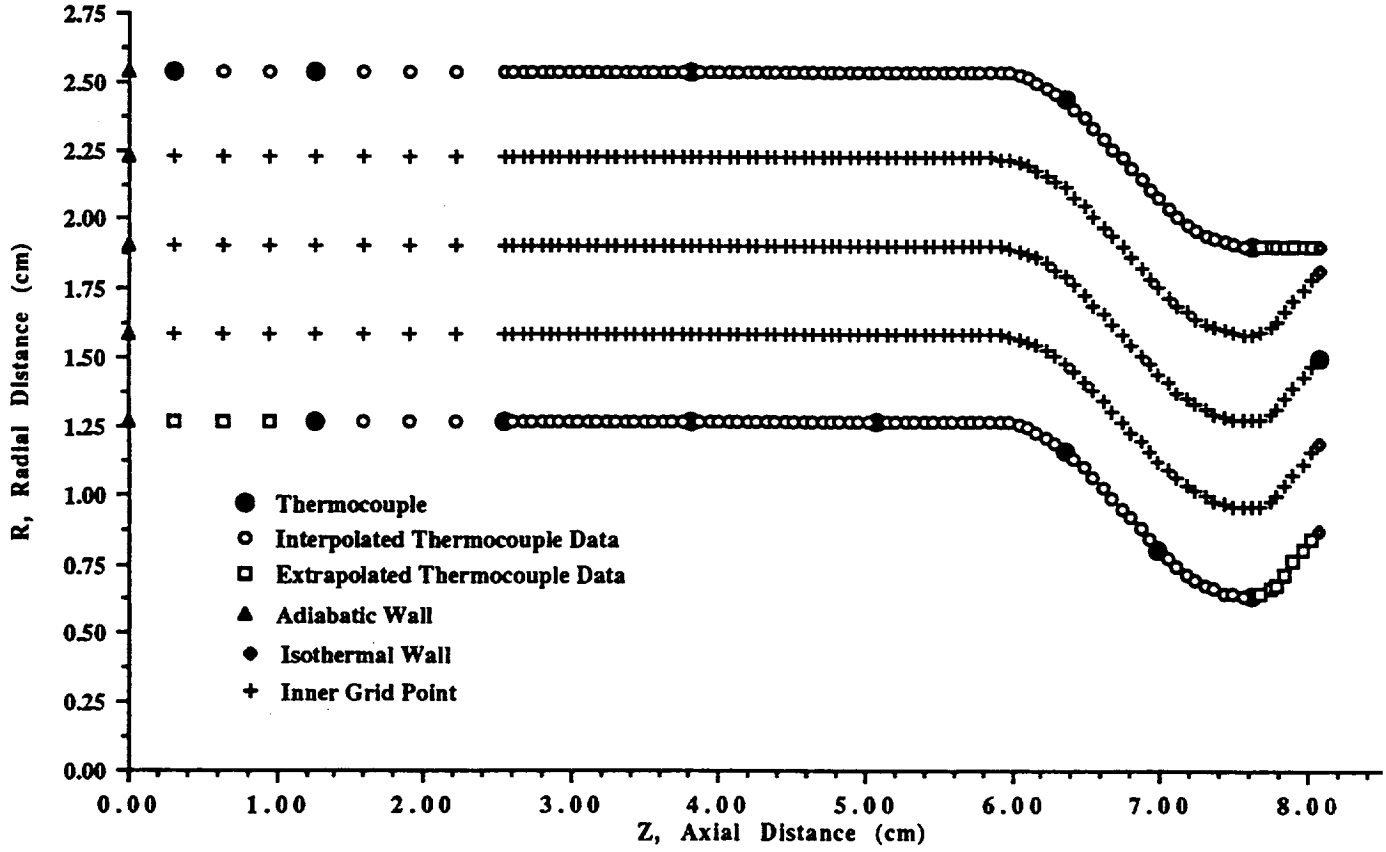

Figure 7: Boundary Condition Definition for Finite Element Model

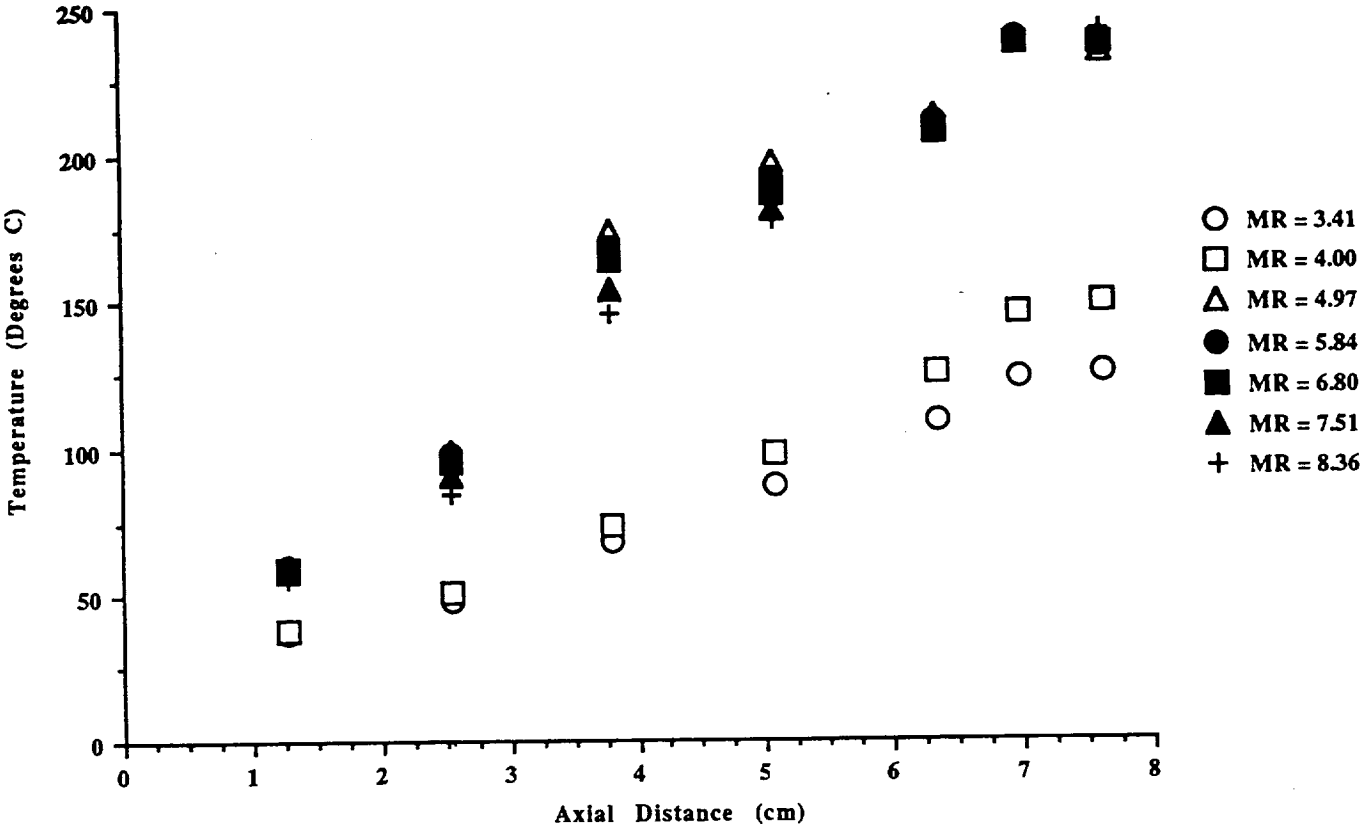

Figure 8: Inner Wall Thermocouple Data

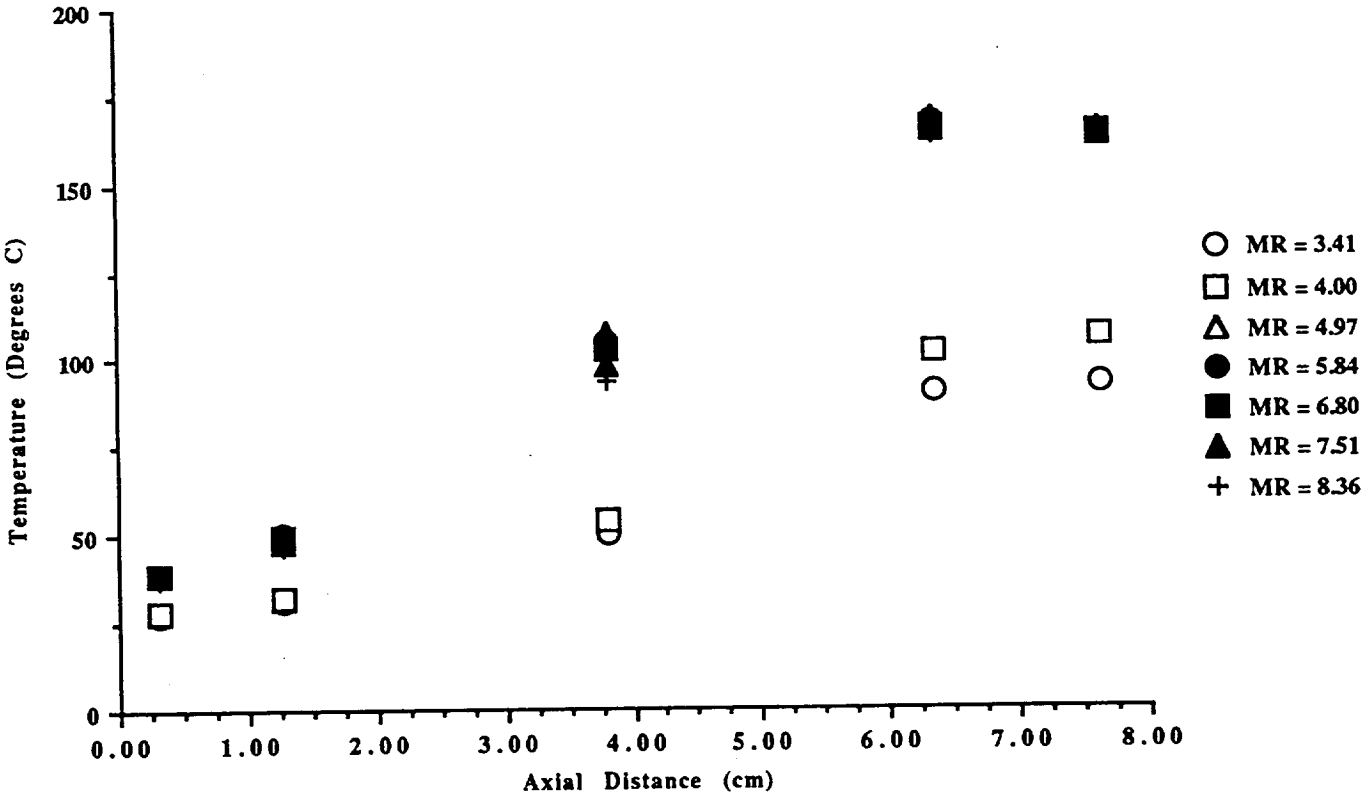

Figure 9: Outer Wall Thermocouple Data

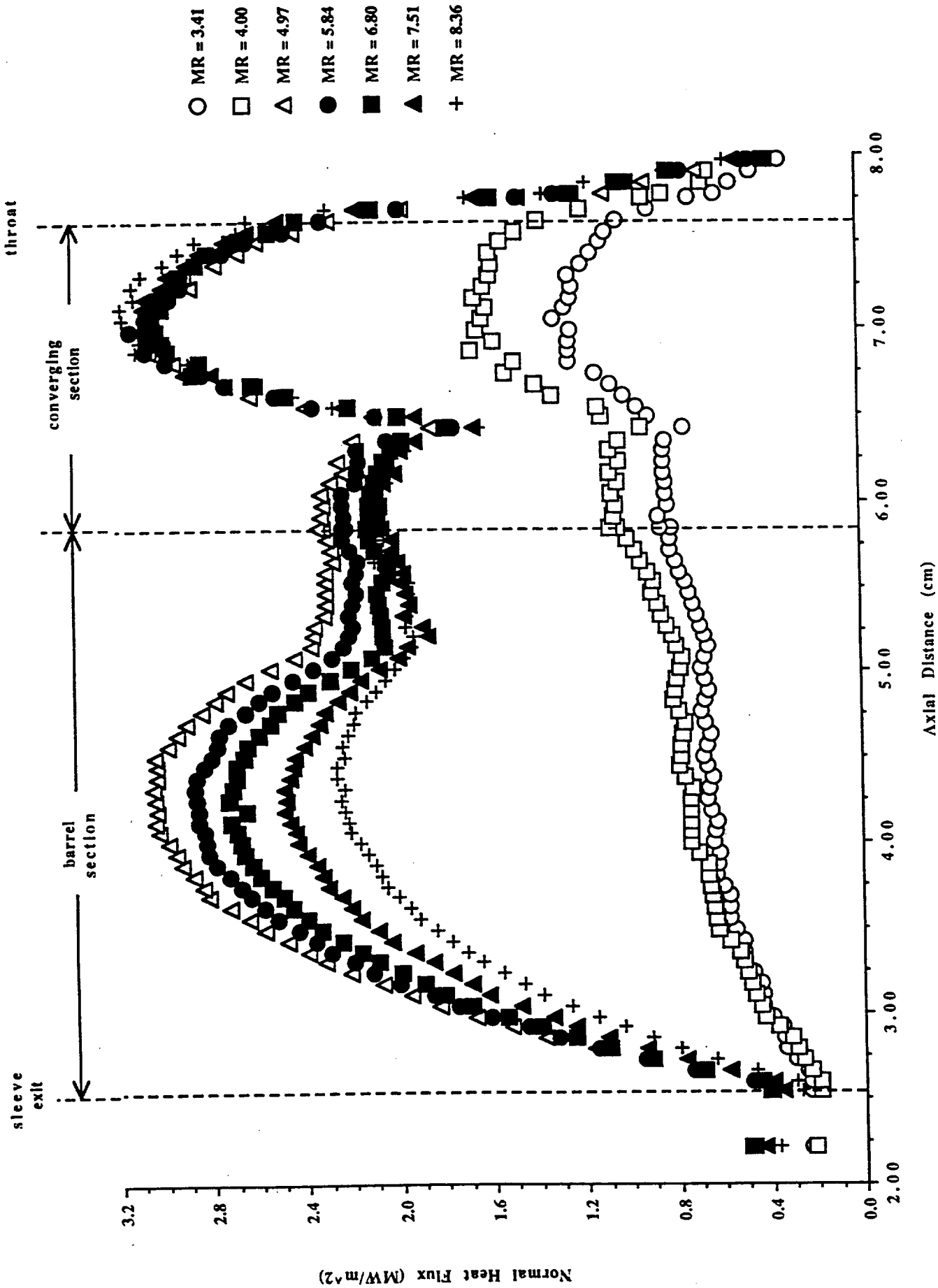

Figure 10: Inner Wall, Normal Heat Flux vs. Axial Distance

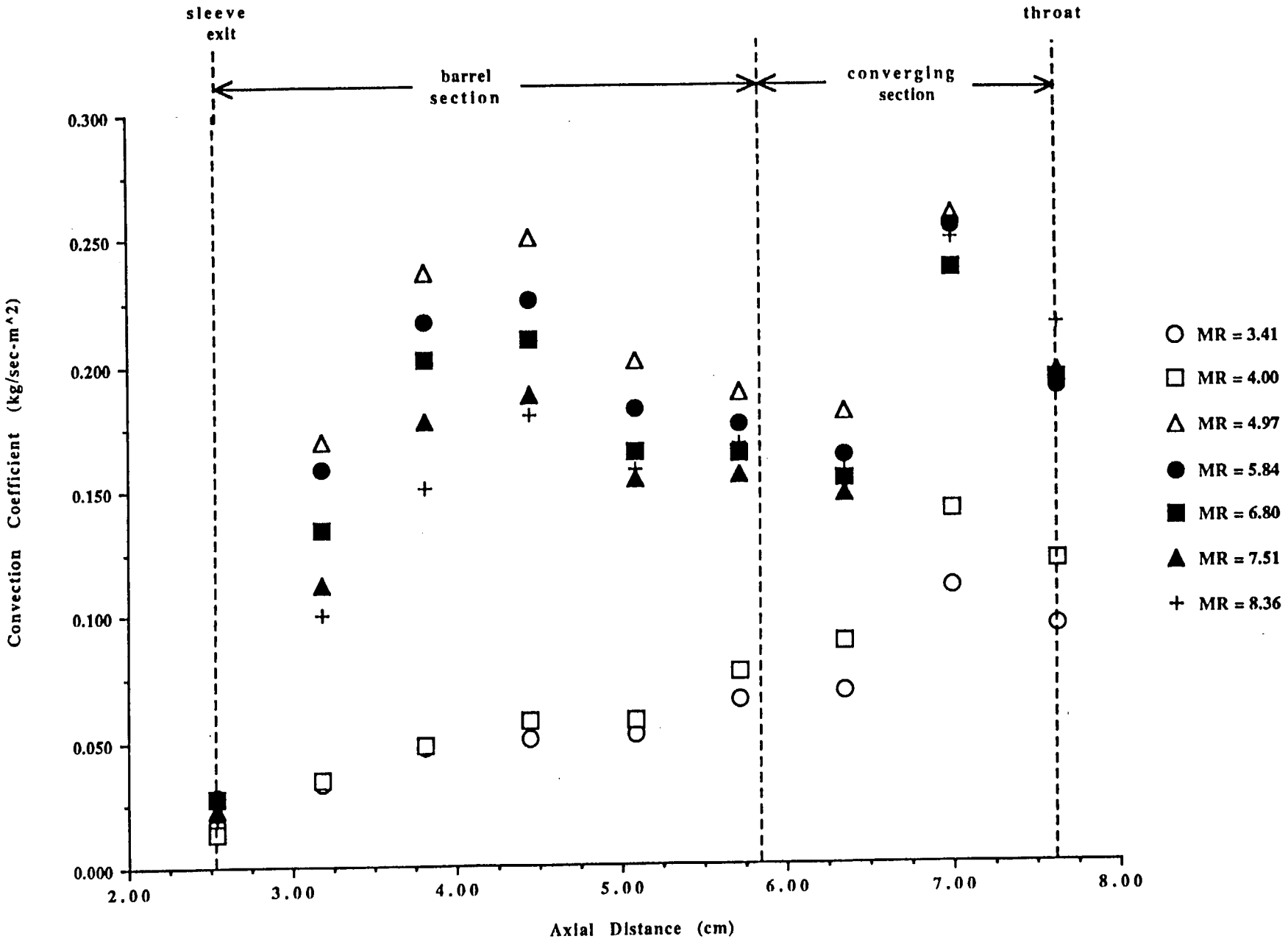

Figure 11: Enthalpy Difference Convection Coefficient vs. Axial Distance

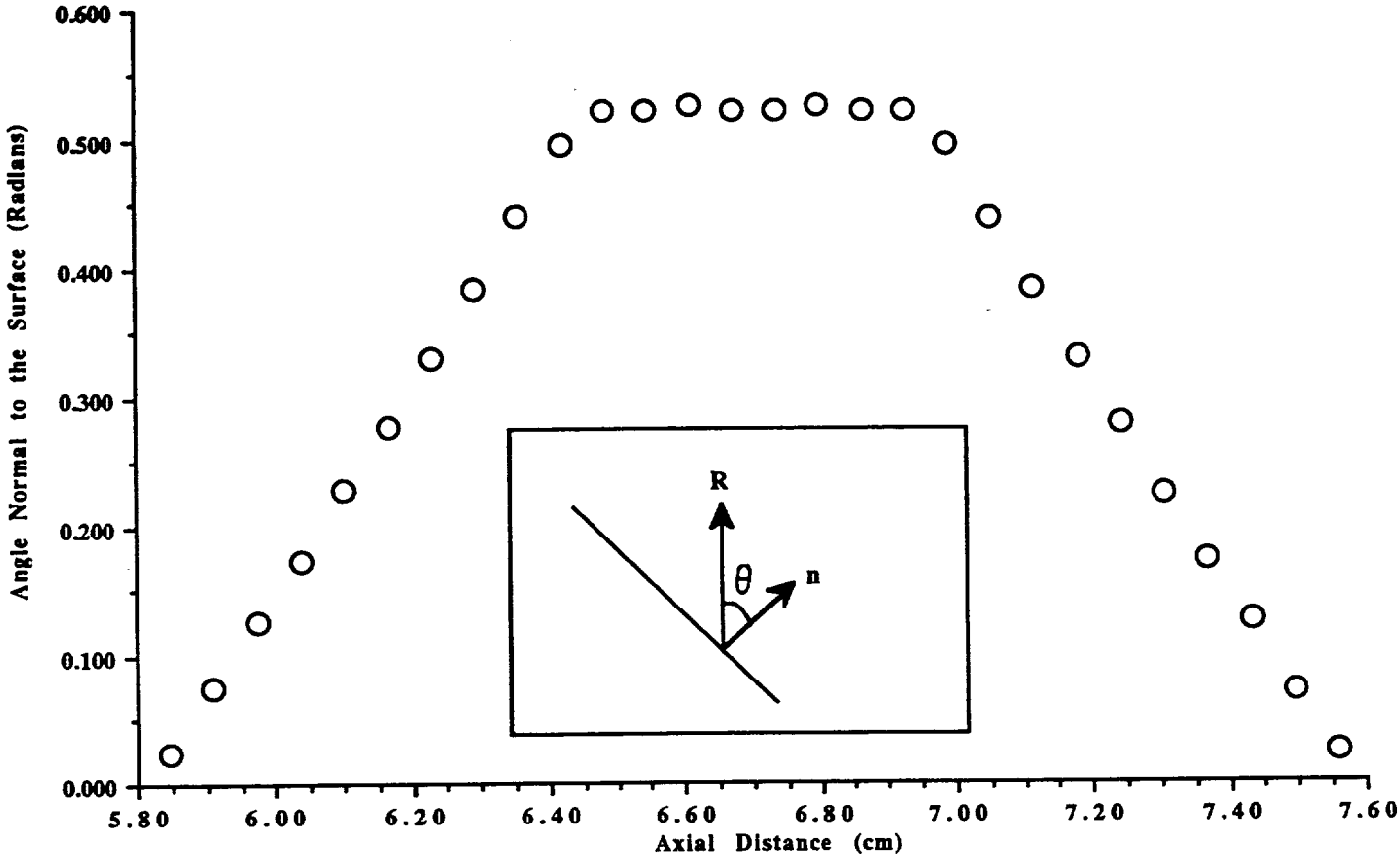

Figure 12: Angle Normal to the Surface (Measured from the Radial Axis) vs. Axial Position

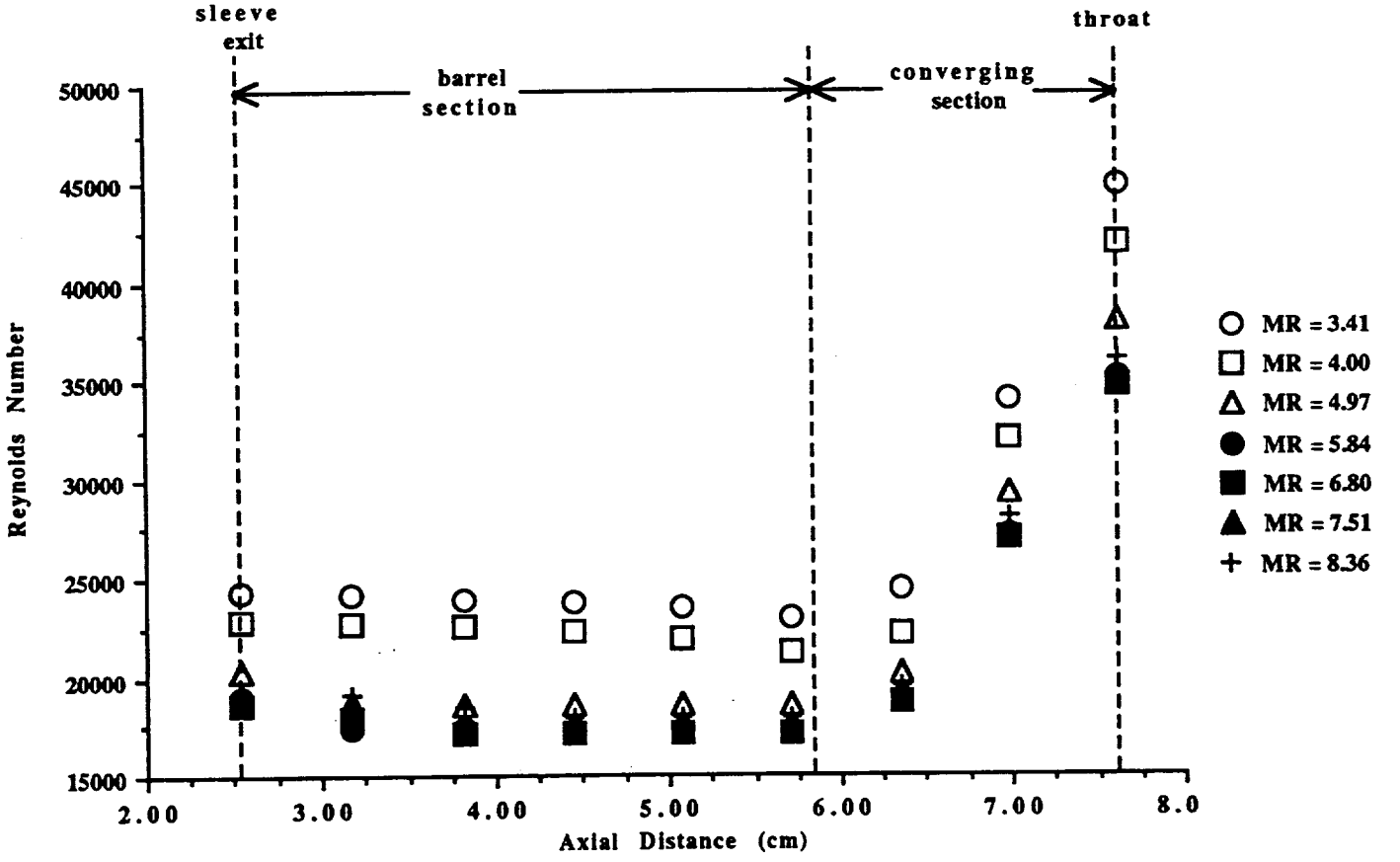

Figure 13: Reynolds Number vs. Axial Distance
Viscosity Evaluated at Reference Properties

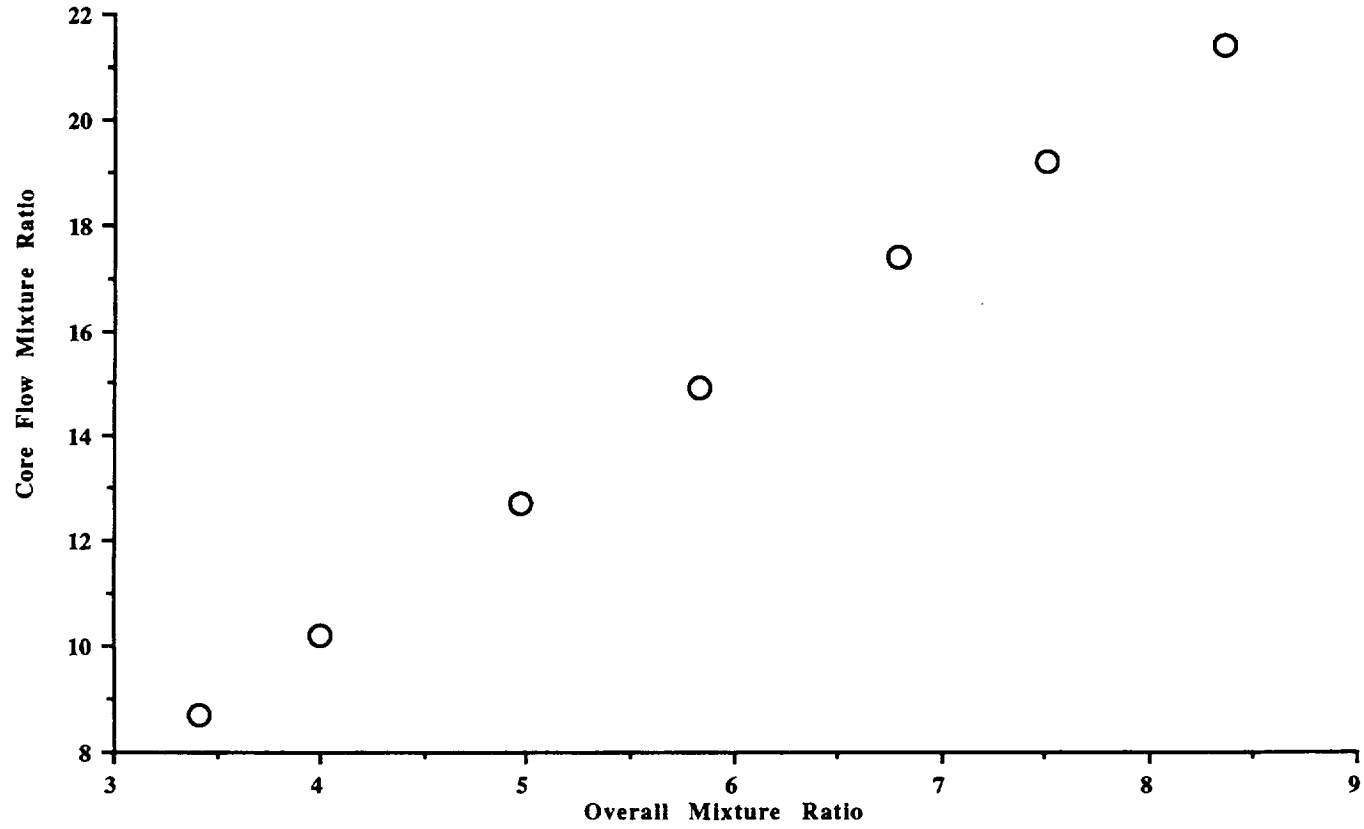

Figure 14: Core Flow Mixture Ratio vs. Overall Mixture Ratio

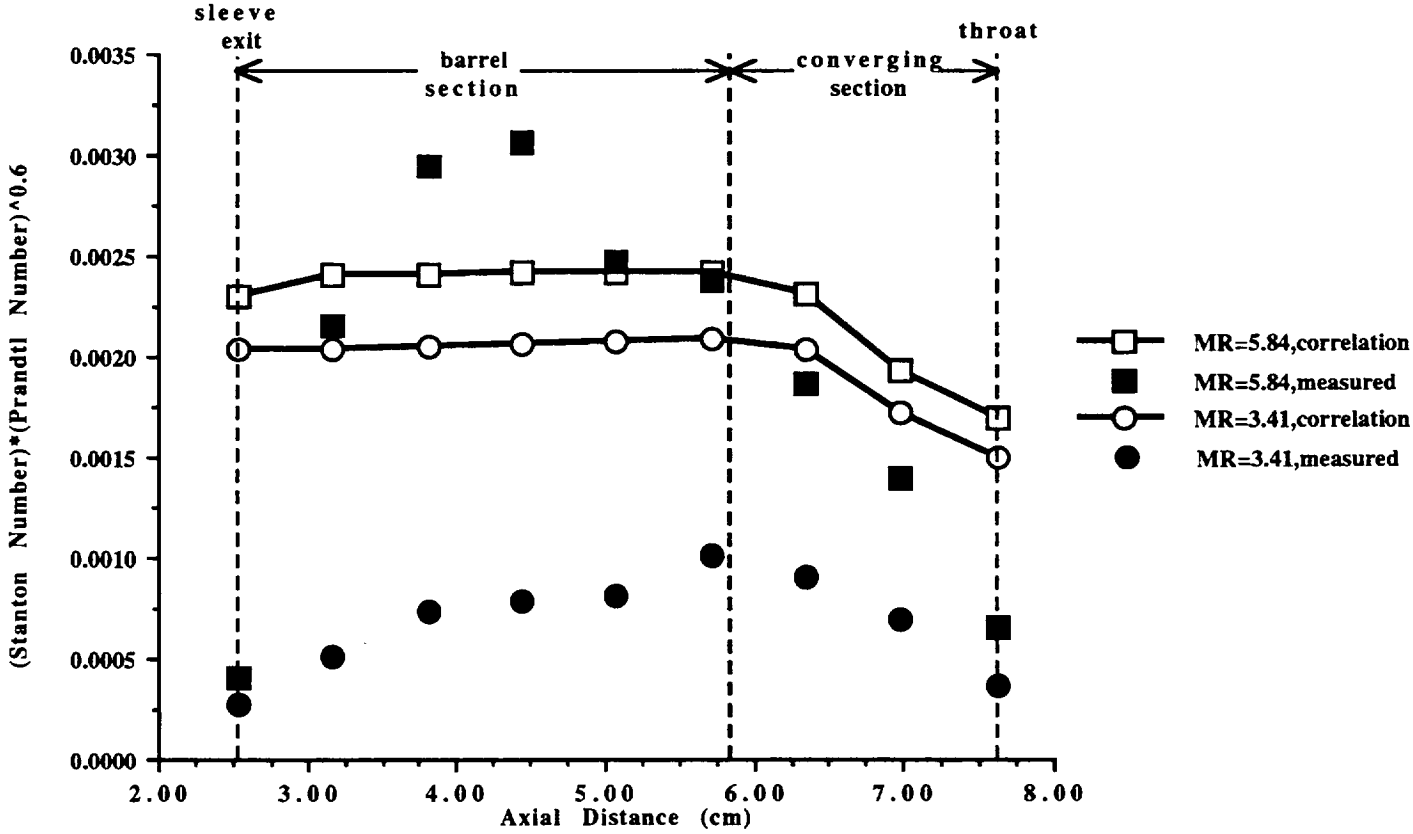

Figure 15: Stanton-Prandtl Grouping Number vs. Axial Distance Laminar Pipe Flow Correlation and Measured Values

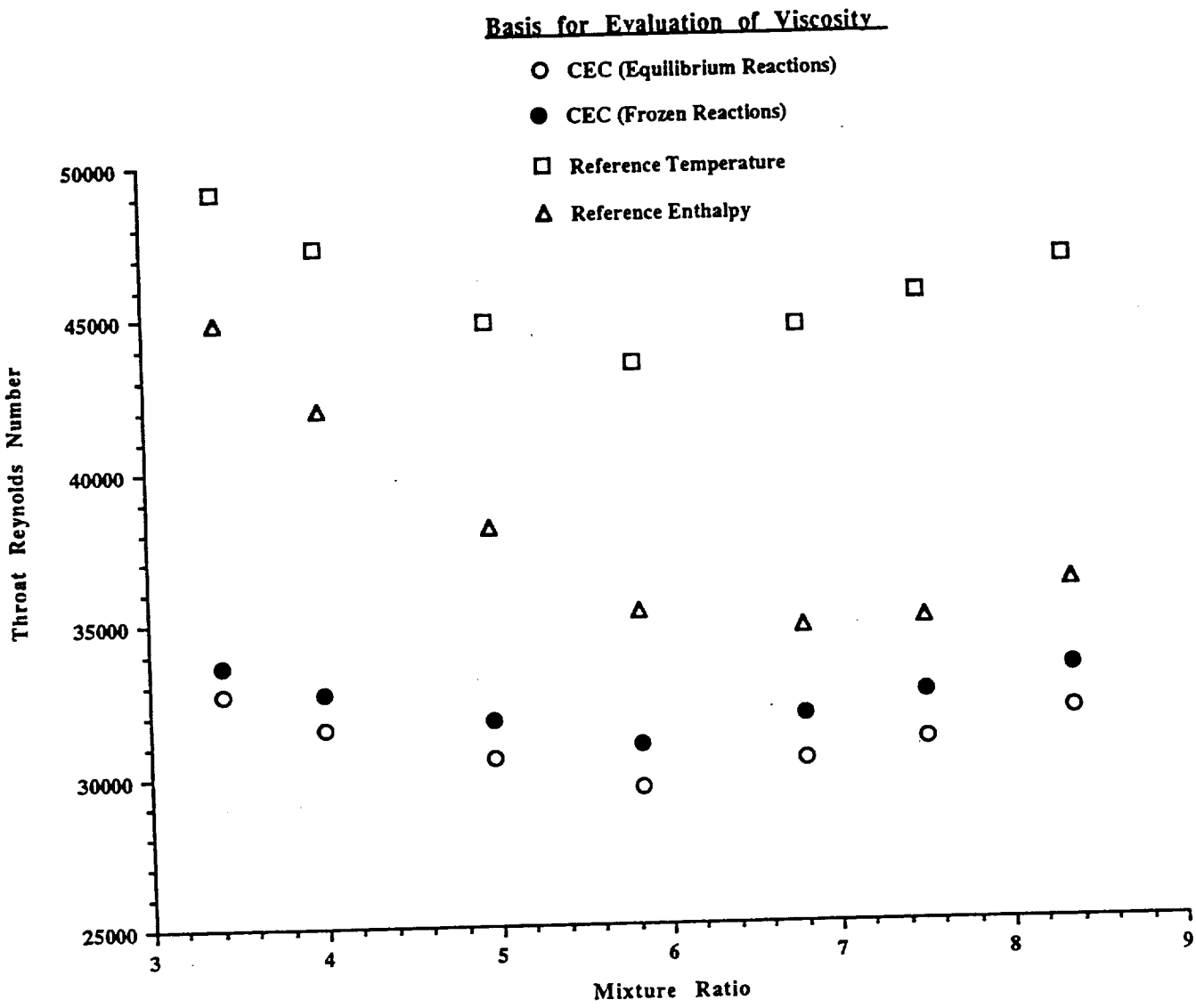

Figure 16: Throat Reynolds Number vs. Mixture Ratio

REPORT DOCUMENTATION PAGE

Form Approved
OMB No. 0704-0188

1. AGENCY USE ONLY (*Leave blank*)	2. REPORT DATE	3. REPORT TYPE AND DATES COVERED
	June 1993	Technical Memorandum

4. TITLE AND SUBTITLE

Small Hydrogen/Oxygen Rocket Flowfield Behavior From Heat Flux Measurements

5. FUNDING NUMBERS

WU-506-42-31

6. AUTHOR(S)

Brian D. Reed

7. PERFORMING ORGANIZATION NAME(S) AND ADDRESS(ES)

National Aeronautics and Space Administration
Lewis Research Center
Cleveland, Ohio 44135-3191

8. PERFORMING ORGANIZATION REPORT NUMBER

E-7953

9. SPONSORING/MONITORING AGENCY NAME(S) AND ADDRESS(ES)

National Aeronautics and Space Administration
Washington, D.C. 20546-0001

10. SPONSORING/MONITORING AGENCY REPORT NUMBER

NASA TM-106233
AIAA-93-2162

11. SUPPLEMENTARY NOTES

Prepared for the 29th Joint Propulsion Conference and Exhibit, cosponsored by the AIAA, SAE, ASME, and ASEE, Monterey, California, June 28-30, 1993. Responsible person, Brian D. Reed, (216) 433-7489.

12a. DISTRIBUTION/AVAILABILITY STATEMENT

Unclassified - Unlimited
Subject Category 20

12b. DISTRIBUTION CODE

13. ABSTRACT (*Maximum 200 words*)

The mixing and heat transfer phenomena in small rocket flowfields with fuel film cooling is not well understood. This study used an instrumented, water-cooled chamber with a gaseous hydrogen/gaseous oxygen injector to gather steady-state inner and outer wall temperature profiles. The chamber was tested at 414 kPa (60 psia) chamber pressure, from mixture ratios of 3.41 to 8.36. Sixty percent of the fuel was used for film cooling. These temperature profiles were used as boundary conditions in a finite element analysis program, MSC/NASTRAN, to calculate the local radial and axial heat fluxes in the chamber wall. The normal heat fluxes were then calculated and used as a diagnostic of the rocket's flowfield behavior. The normal heat fluxes determined for this study were on the order of 1.0 to 3.0 MW/m^2 (0.6 to 1.8 $Btu/sec\text{-}in^2$). In the cases where mixture ratio was 5 or above, there was a sharp local heat flux maximum in the barrel section of the chamber. This local maximum seems to indicate a reduction or breakdown of the fuel film cooling layer, possibly due to increased mixing in the shear layer between the film and core flows. However, the flow was thought to be completely laminar, as the throat Reynolds numbers were below 50,000 for all the cases in this study. The increased mixing in the shear layer in the higher mixture ratio cases appeared not to be due to the transition of the flow from laminar to turbulent, but rather due to increased reactions between the hydrogen film and oxidizer-rich core flows.

14. SUBJECT TERMS

Heat flux; Small rocket flowfields; Gaseous hydrogen/gaseous oxygen rockets; Finite element analysis

15. NUMBER OF PAGES

30

16. PRICE CODE

A03

17. SECURITY CLASSIFICATION OF REPORT	18. SECURITY CLASSIFICATION OF THIS PAGE	19. SECURITY CLASSIFICATION OF ABSTRACT	20. LIMITATION OF ABSTRACT
Unclassified	Unclassified	Unclassified	